Research Square

Preprints are preliminary reports that have not undergone peer review.
They should not be considered conclusive, used to inform clinical practice,
or referenced by the media as validated information.

Quantum Chemical Calculations, Molecular Docking, ADMET and Unveiling Therapeutic Potential of Marine Alkaloid Petrosamine: Shows Promise for Anxiolytic, Anticonvulsant, and Memory-Preserving Effects in Zebrafish Model

Joilna Alves Silva
State University of Ceará
Maria Kueirislene Amâncio Ferreira
State University of Ceará
Antônio Wlisses Silva
State University of Ceará
Emmanuel Silva Marinho
Vale do Acaraú State University
Márcia Machado Marinho
Vale do Acaraú State University
Andreia Ferreira Castro Gomes
Federal University of Ceará
Joana Ribeiro
Federal University of Ceará
Kelma Maria dos Santos Pires Cavalcante
Federal University of Ceará
Otília Deusdenia Loiola Pessoa
Federal University of Ceará
Francisco Chagas Lima Pinto
Federal University of Ceará
Mauro Macedo Oliveira
Universidade Regional do Cariri
Carlos Emidio Sampaio Nogueira
Universidade Regional do Cariri
Jane Eire Silva Alencar Menezes
State University of Ceará

Hélcio Silva Santos

helciodossantos@gmail.com

State University of Ceará

Research Article

Keywords: Petrosamine, Anxiety, Memory, GABAergic, Zebrafish

Posted Date: November 2nd, 2026

DOI: https://doi.org/10.21203/rs.3.rs-11144933/v1

License: This work is licensed under a Creative Commons Attribution 4.0 International License.
Read Full License

Additional Declarations: No competing interests reported.

Quantum Chemical Calculations, Molecular Docking, ADMET and Unveiling Therapeutic Potential of Marine Alkaloid Petrosamine: Shows Promise for Anxiolytic, Anticonvulsant, and Memory-Preserving Effects in Zebrafish Model

Joilna Alves da Silva[a], Maria Kueirislene Amâncio Ferreira[a], Antônio Wlisses da Silva[a], Emmanuel Silva Marinho[b], Márcia Machado Marinho[b], Andreia Ferreira de Castro Gomes[d], Joana Ribeiro[d], Kelma Maria dos Santos Pires Cavalcante[i], Otília Deusdenia Loiola Pessoa[e], Francisco das Chagas Lima Pinto[f], Mauro Macedo de Oliveira[g], Carlos Emidio Sampaio Nogueira[h],Jane Eire Silva Alencar de Menezes[a], Hélcio Silva dos Santos[a,c*]

[a] Laboratory of Chemical-Pharmacological and Environmental Bioassays - LABQFAM, Graduate Program in Natural Sciences, State University of Ceará, Fortaleza, Ceará, Brazil.

[b] Chemistry Course, Vale do Acaraú State University, Sobral, Ceará, Brazil.

[c] Center for Molecular and Environmental Biology, University of Minho, School of Sciences, Department of Biology, Braga, Portugal.

[d] Department of Organic and Inorganic Chemistry, Federal University of Ceará, Campus do Pici s/n, Fortaleza, Ceará, Brazil.

[e] Institute of Exact and Natural Sciences, University of the Integration of Afro-Brazilian Lusophony – UNILAB, Redenção, Ceará, Brazil.

[f] Production Engineering Department, Federal University of the São Francisco Valley - UNIVASF, Salgueiro Campus, Salgueiro, Pernambuco, Brazil.

[g] Departamento de Física, Universidade Regional do Cariri, Juazeiro do Norte, Brazil

[h] University of International Integration of Afro-Brazilian Lusophony, Graduate Program in Sociobiodiversity and Sustainable Technologies, Redenção, Ceará, Brazil

[i] Department of Fisheries Engineering, Center for Agricultural Sciences, Federal University of Ceará, Campus do Pici, Fortaleza, Ceará, Brazil

* Corresponding author: helciodossantos@gmail.com

Abstract

Research into natural products of marine origin has experienced a rapid advance during the 21st century due to the discovery of the various pharmacological potentialities reported in the literature of exclusively marine bioactives with mechanisms of action involving important biological activities found in various species of marine organisms. The pyridoacridine alkaloid petrosamine, extracted from species of sea sponges of the genus *Petrosia sp*., which occur on the coast of the state of Ceará, is a natural marine compound with experimentally proven neuroprotective pharmacological properties. The aim of this article is to evaluate the anxiolytic, sedative, anticonvulsant and memory-preventing effects of the marine alkaloid extract petrosamine in adult *zebrafish*. Thus, the findings confirm the pharmacological potential of petrosamine as an anxiolytic and memory-suppressing agent, supporting its investigation in new therapeutic strategies. Moreover, petrosamine exhibits intermediate chemical reactivity, characterized by a moderate HOMO–LUMO energy gap and high electrophilicity. The MEP and Fukui function analyses consistently highlight the cationic nitrogen atoms as electrophilic centers, while the oxygen and bromine atoms represent the main nucleophilic regions. Petrosamine had a sedative and anxiolytic effect and prevented memory in adult *zebrafish* via GABAergic neurotransmission. The studies evaluated indicate that compounds of marine origin are emerging as a promising source of bioactive compounds, revealing an important therapeutic potential for the treatment of neurodegenerative diseases.

Keywords: Petrosamine, Anxiety, Memory, GABAergic, *Zebrafish*.

Introduction

The vast marine biodiversity represents a natural and sustainable source of biologically active substances that are promising for obtaining raw materials of great pharmacological interest due to their therapeutic properties, especially associated with the treatment of various human diseases[1,2,3].

Due to the genetic diversity of organisms and a unique ecological and molecular diversity, the ocean has been considered an important source of bioactive compounds[4,5,6,7]. In order to adapt to extreme environmental conditions, marine organisms need to produce certain substances vital to their survival that cannot be found in other organisms[8,9,10]. Such compounds sometimes show potent pharmacological activities[2,10].

Most natural marine molecules are produced by invertebrates, such as sponges, corals, bryozoans and ascidians, and belong to different structural classes, such as polyethers, terpenes, alkaloids, macrolides and polypeptides[1,4,5,11].

Currently, several marine natural products have been shown to be effective in experimental models for the treatment of neurological disorders[12,13,14]. The screening and isolation of new molecules with neuroprotective pharmacological properties from marine organisms has gained the attention of the scientific community for the investigation of new therapies with an effect on the pathophysiological events of neurodegenerative diseases that cause significant impairment of neurological functions, often leading to irreversible brain damage[7,13,14].

Alzheimer's, one of the most common neurodegenerative diseases in adults, poses serious threats to health, causing severe damage to neural functions in affected individuals[14,15,16]. The disease is a progressive neurological disorder manifested by cognitive and memory deterioration, marked by the release of neurotoxic and pro-inflammatory factors that intensify neurodegeneration and impair the functioning of the central nervous system[16,17,18]. Its symptoms gradually worsen, which include impaired motor control and some behavioral changes, such as memory and learning deficits, anxiety, agitation and dementia that affect quality of life[7,19].

Studies show that pyridoacridine alkaloids identified and isolated from marine animals have neuroprotective pharmacology, especially with regard to the treatment of Alzheimer's[20,21,22]. An example of a bioactive in this group is the pentacyclic pyridoacridine alkaloid called petrosamine, extracted from the marine sponge of the genus *Petrosia* sp., with a structure based on the 11H pyrido[4,3,2-mn]acridine skeleton and existing in enolate and keto forms[7,20,21]. Through chemical tests, petrosamine showed potent inhibitory action against the enzyme acetylcholinesterase (AChE), which is responsible for degrading the neurotransmitter acetylcholine (ACh) in the synaptic cleft, hydrolyzing it into acetate and choline[20,22,23].

The cholinergic system plays an essential role in learning and memory processes, and dysfunction of this entire process is consistent with the progressive severity of memory impairment observed in

Alzheimer's disease[7,21]. Restoring cholinergic neurotransmission is a useful strategy for increasing synaptic acetylcholine availability and improving impaired memory in patients with the neuropathology[7,24,25].

For the study of biomolecules, the use of zebrafish, also known as zebrafish, in experimental animal models, has stood out on the scientific scene for presenting a good cost-benefit ratio in behavioral and neurophysiological studies to unravel the mechanism of various human diseases, as well as testing new therapeutic agents[26,27,28,29].

As far as the central nervous system is concerned, studies have shown that this animal model contains highly conserved orthologous genes and that despite the lower brain complexity, it has a general organization and neuronal circuits similar to what is observed in mammals, proving to be a model capable of representing human disorders, such as neurodegenerative diseases[30,31,32].

In view of the above, this study aims to investigate the marine alkaloid Petrosamine as a bioactive model to treat diseases that mainly affect the central nervous system, inhibiting neurological disorders in order to contribute to updating data in the scientific literature on marine bioactives and neuropharmacological properties for application against neurodegenerative diseases, as well as evaluating bioassays for anxiety, convulsion, learning and memory in the extract of the marine species *Petrosia* sp.

Materials and Methods

Chemicals and pharmacological agents

All substances employed in the experimental procedures were obtained from commercial suppliers and used without further purification. Diazepam (DZP) was acquired from Neo Química®, donepezil (DNZP) from Geolab®, flumazenil from Sandoz®, dimethyl sulfoxide (DMSO, 3%) from Dynamic®, and pentylenetetrazole (PTZ) from Sigma-Aldrich®. Fresh solutions were prepared on the day of experimentation.

Marine sponge sampling and taxonomic identification

Specimens of the sponge *Petrosia* sp. were collected in March 2014 from the coastal region of Trairí, Ceará State, Brazil (3°13′7.29″ S; 39°15′48.40″ W). A representative voucher (MNRJ 17832) was deposited in the Porifera Collection of the Museu Nacional, Federal University of Rio de Janeiro (UFRJ). Species identification and morphological characterization followed the procedures described by Ribeiro et al. (2024) [33].

Extraction and isolation of the alkaloid

Freshly collected sponge material was immediately immersed in ethanol and stored under freezing conditions until processing. Two independent batches (500 g each) were fragmented and submitted to

ultrasonic-assisted extraction with methanol (2 × 600 mL). After solvent removal under reduced pressure at 40 °C, the resulting hydromethanolic extract was concentrated to approximately 200 mL and subjected to liquid–liquid partitioning with *n*-hexane, dichloromethane (CH_2Cl_2), and ethyl acetate (EtOAc), using three successive extractions (200 mL each solvent). Organic fractions were dried over anhydrous sodium sulfate and evaporated, yielding *n*-hexane (1.4 g), CH_2Cl_2 (0.7 g), and EtOAc (0.2 g) residues. The CH_2Cl_2 fraction was fractionated by size-exclusion chromatography on Sephadex LH-20 using CH_2Cl_2/MeOH (2:8, v/v) as eluent. A blue-pigmented subfraction (213 mg) was further purified by semi-preparative HPLC on a phenylhexyl column employing a linear gradient of H_2O (0.01% TFA)/MeOH (60–100%) over 15 min, at 3.0 mL/min and 35 °C. This procedure afforded petrosamine (45.5 mg; t_R = 10.6 min) with chromatographic purity of 99.1% (Figure S1). Structural identity was confirmed by NMR spectral comparison with published data [20,22] (Figures S2–S6).

Experimental animals and housing conditions

Adult wild-type zebrafish (*Danio rerio*), aged between 90 and 120 days, were used in all in vivo assays. Animals (0.4 ± 0.1 g; 3.5 ± 0.5 cm), of both sexes, were obtained from a commercial supplier in Fortaleza, Ceará, Brazil. Fish were housed in glass aquaria (10 L; density 3 fish/L) under controlled temperature (25 ± 2 °C), neutral pH (7.0), continuous aeration, mechanical filtration, and a 14/10 h light/dark cycle. Commercial Spirulina-based feed was provided until 24 h before experimental procedures. Euthanasia was performed by immersion in ice-cold water (2–4 °C) until complete cessation of opercular movements. All protocols were approved by the Ethics Committee on the Use of Animals of the State University of Ceará (CEUA-UECE; nº 04983945/2021).

Drug administration and experimental workflow

Animals were randomly allocated to experimental groups and gently restrained on a moist sponge for intraperitoneal injections. Treatments consisted of petrosamine (4, 12, or 20 mg/kg), diazepam (4 mg/kg), or vehicle (3% DMSO), administered in a final volume of 20 µL. Injections were performed using 0.5 mL insulin syringes equipped with 30G needles. After administration, each fish was transferred to an individual 500 mL container containing 350 mL of aquarium water and allowed a 30 min recovery period prior to behavioral evaluation [34].

Acute toxicity evaluation, **Locomotor activity analysis and Light/dark preference test**

To assess short-term toxicity, zebrafish (n = 6 per group) received intraperitoneal injections of petrosamine (4, 12, or 20 mg/kg) or vehicle. Animals were observed for 96 h, and mortality was

recorded at 24 h intervals following OECD recommendations [35]. The median lethal dose (LD_{50}) and confidence interval (95%) were calculated using the Trimmed Spearman–Karber method [36].Spontaneous locomotion was evaluated using the open field paradigm to detect alterations in motor performance or sedation [37]. Zebrafish (n = 6 per group) were treated as described above and, after 30 min, individually placed in glass Petri dishes (10 × 15 cm) divided into four equal sectors. The total number of sector crossings was recorded during a 5 min observation period [38].Anxiety-like behavior was assessed using a two-compartment light/dark apparatus consisting of a glass tank (30 × 15 × 20 cm) filled with 3 cm of dechlorinated water [39]. Animals (n = 6 per group) received petrosamine, diazepam, or vehicle and were tested 30 min later. Each fish was introduced into the illuminated compartment, and the cumulative time spent in this area over 5 min was recorded. The dose producing the most consistent anxiolytic-like response was selected for subsequent mechanistic assays [40].

Investigation of GABAergic involvement and PTZ-induced seizure model

To evaluate the participation of GABA_A receptors, zebrafish (n = 6 per group) were pretreated intraperitoneally with flumazenil (4 mg/kg). After 15 min, animals received petrosamine at the previously identified effective dose (12 mg/kg), diazepam, or vehicle. Behavioral assessment was conducted 30 min later using the light/dark test [38]. Anticonvulsant activity was examined using a chemically induced seizure model. Zebrafish (n = 6 per group) were pretreated with petrosamine (4, 12, or 20 mg/kg), diazepam, or vehicle. Thirty minutes later, animals were exposed to PTZ (10 mM), and seizure-like behaviors were classified into three progressive stages: increased swimming activity, circular swimming, and clonic convulsions with transient loss of posture [30,41]. Animals were euthanized immediately after the assessment.

Inhibitory avoidance task

Learning and memory were evaluated using an inhibitory avoidance protocol adapted for adult zebrafish [42]. The apparatus consisted of a two-compartment glass tank (28 × 14.7 × 19 cm) with contrasting black and white areas separated by a sliding partition. The dark compartment was equipped with a grid floor connected to an electrical stimulator. During the training session, fish were placed in the white compartment, and latency to enter the dark area was recorded. Entry into the dark compartment triggered an aversive stimulus (100 Hz, 5 s; 125 mA; 3 ± 0.2 V). Immediately after training, animals received intraperitoneal treatment with petrosamine (4, 12, or 20 mg/kg), diazepam, or vehicle. Memory retention was evaluated 24 h later in a test session identical to training, except that no electrical stimulus was delivered. To investigate the influence of ethanol on memory performance,

an additional experiment was conducted in which zebrafish were exposed to 1% ethanol by immersion for 20 min immediately after training. Animals received the lowest effective dose of petrosamine or vehicle prior to ethanol exposure. Memory retention was assessed after 24 h, following the same protocol described above [43].

Molecular docking simulations

Molecular docking - Anxiolytic and anticonvulsant activity

The two-dimensional representation of the chemical structure of petrosamine was plotted and rendered in the program MarvinSketch® version 24.1.0, Chemaxon© (https://chemaxon.com/marvin), configured to carry out structural optimization using the Merk Molecular Force Field model (MMFF94) with a convergence unit in kcal/mol, parameterized to return only the lowest potential energy confomer[44], used in the molecular docking simulations.For the theoretical evaluation of the anxiolytic and anticonvulsant activity of petrosamine, we followed the methodology of Mendes et al. (2022)[41], where the structures of the proteins were obtained from the RCSB Protein Data Bank server (https://www.rcsb.org/) and prepared for molecular docking simulations using the AutoDockTools program™ version 1.5.6 - MGL Tools© (https://autodock.scripps.edu/). The structure of carbonic anhydrase II (CAII), identified as 'Coumarins are a novel class of suicide carbonic anhydrase inhibitors', classified as a lyase in *Homo sapiens* organism (resolution of 2.0 Å) is deposited on the server under PDB code 3F8E[45], while the structure of the GABA receptor$_A$ R, identified by 'CryoEM structure of human full-length alpha1beta3gamma2L GABA(A)R in complex with diazepam (Valium), GABA and megabody Mb38' and classified as a membrane receptor in the organisms *Homo sapiens* and *Escherichia coli* (resolution of 3.58 Å), is deposited in the database under the PDB code 6HUP[46]. The polar hydrogens and Gasteiger charges were added to the protein structure in the AutoDockTools program™. The grid-box was delimited to cover the entire conformational space of the proteins, adjusted to the dimensions 50Åx47Åx60Å (x,y,z) and coordinates x = -6.650, y = -0.180 and z = 16.240, for the CAII enzyme, and to the dimensions 129Åx99Åx125Å (x,y,z) and coordinates x = 125.282, y = 139.530 and z = 136.020, for the GABA receptor$_A$ R. The AutoDockVina code™ was configured to perform a series of 50 independent simulations of 20 poses each, applying the Lamarkian Genetic Algorithm (LGA), for the ligand petrosamine and the co-crystallized ligands TE1 (CAII inhibitor), Diazepam (DZP - GABA$_A$ R agonist)[47]. The choice of the *best-pose* involves the evaluation of energetic and statistical parameters, provided that they are within predefined ideal limits: an affinity energy below -6.0 kcal/mol and a *Root Mean Square Deviation* (RMSD) of less than 2.0 Å[48].

Molecular docking – inhibitor AChE

The production of the molecular docking simulations of AChE inhibitors followed some essential steps regarding the preparation of all the components evaluated in the simulations. Among the compounds used was galantamine (GNT), classified as a crystallised AChE inhibitor, while the biocompound petrosamine was analysed for the drug candidate compound. Both compounds were rendered using the software Marvinsketch® version 25.1.0, Chemaxon© (https://chemaxon.com/marvin)[49] determined the two-dimensional structures of each structure, then the compounds were sent to the software Avogadro® version 1.2.0[50], with the aim of structurally optimising the respective compounds in order to achieve the lowest energy state when the force field is applied MMFF94 (Merck Molecular Force Field 94)[51], in order to obtain the most stable structures in terms of the force field metrics used[52]. The crystal structure of acetylcholinesterase obtained for the molecular docking prediction studies was obtained using the Protein Data Bank virtual platform using the identification code IDpdb: 4EY6, the crystal structure is labelled "Crystal Structure of Recombinant Human Acetylcholinesterase in Complex with (-)-galantamine", this biological receptor is classified as a hydrolase, linked to the *Homo sapiens* organism, showing no mutations in its three-dimensional coordinates; the resolution of the structure was realised using the X-ray diffraction method, showing a resolution equal to 2.40 Å[53,54]. In order to proceed with the molecular docking prediction studies, the crystallised structure needs to go through a preparation process in order to obtain the ideal, standardised structure, the first step is to use the software Chimera[55,56], using the programme, it is possible to remove all the residues present in the coordinates of the target receptor, consisting of water molecules and ligands; after cleaning the receptor, the structure is sent to the software AutoDockTools[57], where all the hydrogens in each amino acid present in the enzyme chain were added, then all the *Gasteiger* charges were computed[58]. Finally, the GridBox values specific to the AChE target were determined, with the coordinate axes equal to (-0.420 x, -51.390 y, 4.105 z) and size (90 x, 91 y, 126 z), these values being used to consider the entire receiver in the prediction studies. The molecular docking simulations are based on the individual use of each ligand in relation to the target receptor. 50 independent simulations were carried out for each complex, where 20 poses formed between the ligand and protein are available for each one, prediction studies were carried out using the software AutoDockVina[57,59]. The determination of the best poses is linked to the complex formation parameters based on the RMSD value and affinity energy, with values equal to or less than 2.0 Å (RMSD) and -6.0 kcal/mol (energy)[52].

MPO-based ADME study

In order to predict the druglikeness properties and absorption, distribution, metabolism and excretion (ADME) descriptors, the physicochemical attributes of petrosamine were analyzed based on the Central Nervous System Multiparameter Optimization (CNS MPO) algorithm, as shown in Eq. 1:

$$d = \sum_{i=1}^{N} w_k \left(T(x^0)\right)_k \qquad (1)$$

where *w* is the weighting factor (0 to 1) of each physicochemical attribute (*k*), assigned to the function of satisfying the statistical thresholds ($T(x)$), which include: intrinsic lipophilicity (logP) ≤ 3 and at physiological pH (logD at pH 7.4) ≤ 2, molecular weight (MW) ≤ 360 g/mol, topological polar surface area (TPSA) 40-90 Å², H-bond donors (HBD) ≤ 1 and basic pKa ≤ 8 (N = 6 properties), and the sum results in the desirability score (*d*) which ranges from 0 to 6 according to ADME viability. The physicochemical properties were calculated in the ADMETlab 3.0 predictor (https://admetlab3.scbdd.com/) and analyzed according to the Pfizer rule classification system[60] and Golden Triangle rule[61], based on graphic signatures[62]. The results were related to the ADME descriptors associated with oral absorption and metabolic stability provided by the ADMETlab 3.0 (https://admetlab3.scbdd.com/) and Deep-PK (https://biosig.lab.uq.edu.au/deeppk/)[63], which include apparent permeability (P_{app}) in MDCK cells, intestinal P-glycoprotein (P-gp) substrate, volume of distribution (VD), access to the central nervous system (CNS) by permeability at the blood-brain barrier (BBB) and intrinsic hepatic clearance rate ($CL_{int,u}$). Petrosamine metabolism sites were predicted using the SMARTCyp server (https://smartcyp.sund.ku.dk/mol_to_som), based on a similarity test of the input compound with fragments known to be substrates of cytochrome P450 (CYP450) isoforms, where the results were related to toxicity descriptors based on drug-induced liver injury (DILI) and mutagenicity, present on the ProTox 3.0 server (https://comptox.charite.de/protox3/).

Statistical analysis

Results were expressed as mean values ± standard error for each group of 6 animals. After confirming the normality of the distribution and homogeneity of the data (Shapiro-Wilk test), the differences between the parametric groups were identified using one-way ANOVA analysis of variance for the OFT test and two-way ANOVA for the anxiolytic mechanism of action tests, convulsive behavior test and inhibitory avoidance. The non-parametric data from the LDT test was analyzed using the Kruskal-Wallis test followed by the Dunn and two-way post hoc tests. All analyses were carried out using the GraphPad Prism v. 8.0 program. The level of statistical significance was set at 5% ($p<0.05$).

Theoretical studies of chemical reactivity

Reactivity at the molecular level lies at the heart of chemical science. Reactivity theories comprise a set of principles that relate molecular structure to the capacity to donate or accept electrons

[107].There are two classes of chemical reactions: charge-controlled and orbital-controlled. In orbital-controlled reactions, stabilization arises from the transfer of electrons from the highest occupied molecular orbital (HOMO) to the lowest unoccupied molecular orbital (LUMO). This occurs because that interaction incurs the lowest energy penalty[108]. In Density Functional Theory (DFT), the electronic energy is a functional of the electron density $\rho(r)$, and by analyzing the response of $E(\rho)$ to variations in the number of electrons N and the external potential $v(r)$, global and local descriptors that quantify chemical reactivity emerge [109]. In this study the molecular geometry optimization and orbitals energies of the isolated molecule was carried out using Density Functional Theory – DFT[110] with wb97xd hybrid functional[111] and GENECP (SDD for Br and 6-31G++(d,p) for all others) basis set specification. The geometric parameters and boundary molecular orbital energy (HOMO and LUMO) were duly obtained from the optimised structure. Thus, the global reactivity descriptors were predicted using the equations[112]:

$$GAP\ Energy: \Delta E_{GAP} = E_{HOMO} - E_{LUMO} \quad (2)$$

$$Ionization\ Energy: I = -E_{HOMO} \quad (3)$$

$$Electron\ Affinity: A = -E_{LUMO} \quad (4)$$

$$Electronegativity: \chi = -\frac{(E_{HOMO} + E_{LUMO})}{2} \quad (5)$$

$$Chemical\ Hardness: \eta = \frac{(E_{LUMO} - E_{HOMO})}{2} \quad (6)$$

$$Chemical\ Softness: \sigma = \frac{1}{\eta} \quad (7)$$

$$Electrophilicity: \omega = \frac{\chi^2}{2\eta} \quad (8)$$

The Fukui function $f(r)$ is a local reactivity descriptor that shows where the electron density most respond to the addition or removal of electrons, thereby linking frontier orbital theory to DFT. The Fukui function is defined as

$$f(r) = \left[\frac{\partial \rho(r)}{\partial N}\right]_{v(r)} = \left[\frac{\delta \mu}{\delta v(r)}\right]_N \quad (9),$$

that is, as local change in electron density with respect to a charge in the number of electrons at fixed external potential or, equivalently, it quantifies the sensitivity of the chemical potential to a localized external perturbation. Intuitively, $f(r)$ highlights reactive sites, large values indicate regions more prone to accept or donate density in chemical processes, generalizing the frontier orbital concept. For nucleophilic attack, $f^+(r) = \left[\frac{\partial \rho(r)}{\partial N}\right]^+_{v(r)} \approx \rho_{(N+1)}(r) - \rho_N(r)$ (10) (electron addition), for electrophilic attack $f^-(r) = \left[\frac{\partial \rho(r)}{\partial N}\right]^-_{v(r)} \approx \rho_N(r) - \rho_{(N-1)}(r)$ (11) (electron removal), and for radical attack $f^0(r) = \left[\frac{\partial \rho(r)}{\partial N}\right]^0_{v(r)} \approx \rho_{(N+1)}(r) - \rho_{(N-1)}(r)$ (12).

In this work, the numerical Fukui function values were approximated using the Hirshfeld-condensed Fukui approximation, which computes atomic Fukui indices as finite differences of Hirshfeld charges evaluated at the three charge states (N, N+1 and N-1). Therefore, $f_k^+ = q_k(N+1) - q_k(N)$ (13), $f_k^- = q_k(N) - q_k(N-1)$ (14) and $f_k^0 = q_k(N+1) - q_k(N-1)$ (15). This approximation is valid when the frontier-electron picture is adequate, the N ± 1 species are well-behaved (bound or effectively stabilized), and all three calculations use the same level of theory so that population differences reflect genuine response rather than methodological inconsistency[112-114].

Molecular electrostatic potential (MEP)

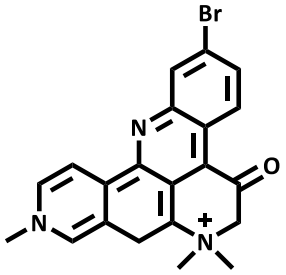
The electrostatic potential V(r) is defined as the contribution of electrons and nuclei to the space around the molecule. It is a rigorous property that can be obtained both experimentally and through quantum chemistry. In standard notation, $V(r) = \sum_{i=1}^{N} \frac{Z_i}{|R_i - r|} - \int \frac{\rho(r')}{|r' - r|} dr'$ (16), where Z_i is the charge on the nucleus (i) located at R_i and $\rho(r')$, the electron density is found at a point r' near the given molecule. This equation highlights the dependence of V(r) on both the nuclear distribution and the computed electron density[115]. Therefore, after the DFT calculations, which provide the electron density ρ(r) and the geometry/electronic states of the optimized structure, the MEP was calculated from the self-consistent electron density and nuclear positions, evaluating the classical potential at points in space.

Results

Structural Analysis

The marine alkaloid petrozoamine was isolated as dark blue needles, showing a melting point of 330–332 °C. The UV-PDA spectrum (H_2O/MeOH) exhibited absorption maxima at 286, 345, and 589 nm, typical of highly conjugated aromatic systems present in marine phenazinone-type alkaloids. The ^{1}H NMR spectrum (300 MHz, MeOD, Figure S2) revealed several diagnostic resonances confirming the aromatic and methoxy-substituted structure of petrozoamine. A singlet at δH 9.80 (1H, H-9) corresponds to a deshielded aromatic proton adjacent to a carbonyl or heteroatom. Two doublets at δH 9.45 (1H, J = 5.7 Hz, H-12) and δH 9.05 (1H, J = 5.7 Hz, H-11) indicate ortho-coupled aromatic protons within a 1,2-disubstituted ring. Additional aromatic signals were observed at δH 9.13 (1H, J = 9.0 Hz, H-4) and δH 7.78 (1H, J = 9.0 Hz, H-3), consistent with another ortho-coupled pair, while a broad singlet at δH 8.29 (1H, H-1) is typical of an isolated aromatic proton in a heteroaromatic system. The aliphatic region displayed a singlet at δH 4.63 (2H, H-6), attributed to a benzylic methylene group,

and three singlets at δH 4.67 (3H, Me-14) and δH 3.93 (6H, Me-15 and Me-16) corresponding to one N-methyl and two methoxy substituents, respectively. The ^{13}C NMR spectrum (75 MHz, MeOD, Figure S3) confirmed the presence of a highly conjugated aromatic system. The signal at δC 188.1 (C-5) corresponds to a carbonyl carbon, while the resonance at δC 162.5 (C-8) indicates an aromatic carbon attached to oxygen. Several downfield signals between δC 146.7–141.2 (C-9, C-13a, C-12b, C-11, C-12a) represent quaternary carbons adjacent to heteroatoms. Additional aromatic carbons appeared between δC 136.7–116.3, consistent with a polycyclic aromatic core. The benzylic carbon at δC 72.0 (C-6), methoxy carbons at δC 54.7/54.5 (C-15 and C-16), and an N-methyl carbon at δC 49.3 (C-14) further support the proposed substitution pattern. Together, these spectral data are fully consistent with the structure of petrozoamine, a marine-derived alkaloid (Ribeiro et al. 2024) [33]..



Marine Alkaloid Petrosamine

Acute toxicity in adult *zebrafish*

It was shown that the 4 mg/kg, 12 mg/kg and 20 mg/kg doses of petrosamine were not toxic to adult *zebrafish* up to 96 h after analysis (LD_{50} > 40 mg/kg), as there was no death and no apparent anatomical changes in the animals during this period ($p < 0.05$).

Assessment of locomotor activity (open field test - OFT)

The open field test serves as a behavioral parameter used to evaluate the action of drugs that can affect the central nervous system of adult *zebrafish*, taking into account the animal's swimming activity, as well as its movement to analyze if there has been a restriction of locomotion, resulting in a more static animal or if the swimming continues with the regular pattern[64,65].

In this test, the animals perform exploratory behaviors, including tigmotaxis, exploratory swimming, bouts of cong elation and erratic movements[66]. In this task, *zebrafish* initially exhibit high levels of activity, which shows intra-session habituation[67]; in addition to this aspect of non-associative learning, *zebrafish* also show aspects of fear[66,68], with a tendency to spend most of their time swimming close to the walls of the tank, making short-lived forays into the center of the aquarium[64].

One-way ANOVA analysis revealed that the alkaloid petrosamine did not cause locomotor impairment at the lowest doses (4 and 12 mg/kg), unlike the effects of diazepam ($^{\#}p<0.05$, $^{\#\#\#}p<0.001$ vs. DZP). This demonstrates that petrosamine does not alter locomotion at low doses. However, at a dose of 20 mg/kg, the fish exhibited behaviour similar to that of the diazepam group, displaying lethargic locomotion (Figure 1). All doses produced behaviour that differed from that of the control group (DMSO 3%; *p<0.05, ***p<0.001, ****p<0.0001 vs. control).

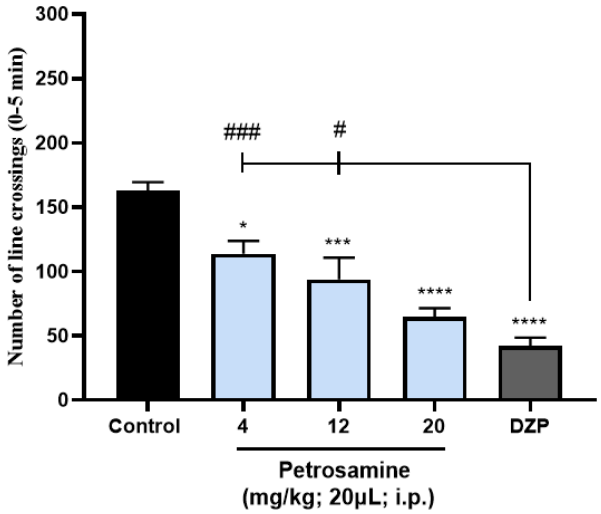


Figure 1. Effect of petrosamine on locomotor behavior of adult *zebrafish* in the Open Field Test (0-5 min). Each column represents the mean ± standard error of the mean (n= 6 groups). Control: DMSO 3.0%; 20 µL, *i.p.* One-Way ANOVA followed by Tukey's test: (*p<0.05, ***p<0.001, ****p<0.0001 vs Control; the bristle indicates statistical significance compared to the DZP -Diazepam group, $^{\#}p<0.05$, $^{\#\#\#}p<0.001$ vs DZP).

Anxiolytic Assessment (Light/dark test - LDT)

Anxiety assessment can be seen in experimental animal models, representing a natural emotional response to potentially threatening situations, such as exposure to novelty, predator odor or other threatening contexts[69,70,71].

Zebrafish are increasingly used in translational studies of stress and anxiety, as well as in central nervous system (CNS) drug screening[72,73] because they exhibit high genetic homology with humans, with approximately 70% of human genes having at least one *zebrafish* orthologue[74] and exhibit robust anxiety-like behaviors[75,76] that are highly sensitive to various genetic[71], epigenetic[77,78,79], neuropharmacological[80] and environmental factors[81,82,83].

Similar to diazepam, petrosamine significantly (*p<0.05, ***p<0.001 vs Control) reduced the anxious behavior of adult zebrafish at the tested doses (12 and 20 mg/kg). The animals spent more time in the clear zone of the aquarium than the negative control (vehicle: DMSO 3%). A dose-

dependent effect of petrosamine was observed: the highest dose (20 mg/kg) was the most effective in inducing anxiolytic behavior in the animals (Figure 2).

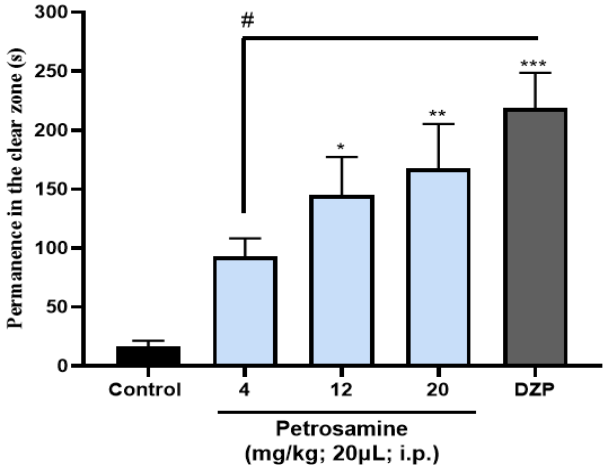


Figure 2. Effect of petrosamine on the anxiety behavior of adult *zebrafish* in the light and dark test (0-5 min). Control group (DMSO 3%; 20 µL; i.p.); DZP - Diazepam (4 mg/kg; 20 µL; i.p.). The values represent the mean ± standard error of the mean for 6 animals/group; ANOVA followed by Turkey's test (*$p<0.05$; **$p<0.01$ vs. Control; the bristle indicates statistical significance compared to the Diazepam group, $^{\#}p<0.05$ vs. DZP).

Assessment of GABAergic neuromodulation ($GABA_A$ receptor)

The GABAergic system is the main route of action of anxiolytic herbal medicines[84,85], since gamma-aminobutyric acid (GABA) is the main inhibitory neurotransmitter present in the central nervous system of mammals[86,87].

Zebrafish are widely used to understand the effects of pharmaceuticals on anxiety-related stress, behavior and physiology due to their conserved behavioral, neuroanatomical, pharmacological and transcriptional stress responses in mammals and other species[75,88].

We evaluated the interaction between petrosamine and the $GABA_A$ receptor using flumazenil, a $GABA_A$ receptor benzodiazepine antagonist, as a pretreatment. A two-way ANOVA test revealed that flumazenil blocked the anxiolytic effect of petrosamine (20 mg/kg; i.p.) ($^{\#\#\#\#}p<0.001$ vs. Petrosamine), interfering with the amount of time that zebrafish spent in the clear zone of the aquarium. This result was similar to that observed in the group pretreated with flumazenil (4 mg/kg) and diazepam (4 mg/kg). These animals spent most of their time in the dark region of the light-dark test ($^{\#\#\#\#}p<0.001$ vs. DZP) (Figure 3).

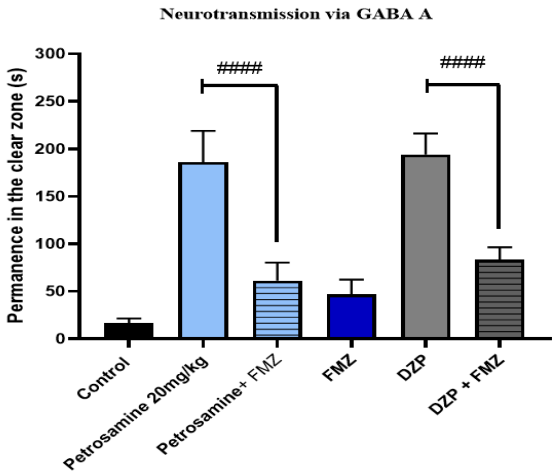


Figure 3. GABAergic mechanism of action of petrosamine (20 mg/kg) on the anxiety behavior of adult *zebrafish* in the light and dark test (0–5 min). Grupo controle (DMSO a 3 %); DZP – Diazepam (4 mg/kg; 20 µL; i.p.), flumazenil (4 mg/kg; 20 µL; i.p.). The values represent the mean ± standard error of the mean for 6 animals/group; ANOVA followed by Turkey's test (*p<0.05; ****p<0.0001 vs. Control; the bristle indicates statistical significance compared to the Fmz + DZP group, ####p<0.0001).

Evaluation of seizures induced by pentylenetetrazole (PTZ)

One of the most widely used approaches to induce seizures in animals are chemoconvulsants, such as pentylenetetrazole (PTZ)[89]. When administered PTZ, zebrafish progress through a distinct set of movements and postures that end with generalized tonic-clonic seizures[90,91]. PTZ is believed to induce seizures mainly by binding to the γ-aminobutyric acid receptor ($GABA_A$), preventing the neuroinhibitory action of GABA[90,91].

In evaluating the three stages of pentylenetetrazol (PTZ) -induced seizures, the 12 mg/kg dose of petrosamine, had a similar effect to diazepam (DZP) in stages I and II (****p<0.0001, **p< 0.01 vs. control), and a partial effect in stage III (*p<0.05 vs. Control; ##p<0.05 vs. Diazepam). Diazepam reversed the convulsive behavior in all three stages (****p<0.0001 vs. control) when compared to the control group (Figure 4).

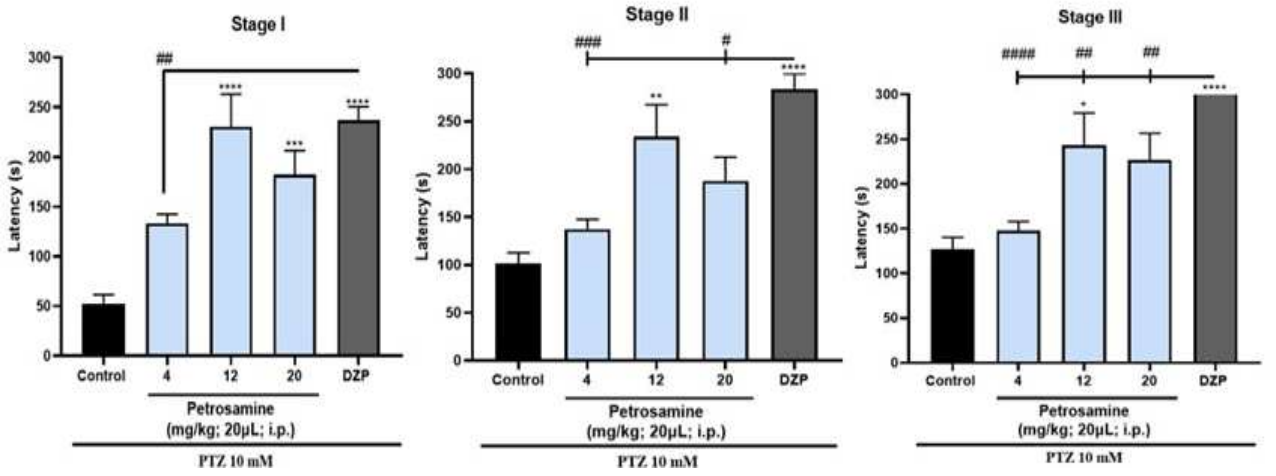


Figure 4. Effect of petrosamine (i.p.) on seizure induced by pentylenetetrazol (10 mM) in adult zebrafish, stage I (A), stage II (B) , stage III (C). Control group (DMSO at 3%); DZP - Diazepam (4.0 mg/kg; 20 µL; i.p.). Values represent the mean ± standard error of the mean for 6 animals/group; data were expressed as two-way ANOVA. * indicate statistical significance in comparison with control, and # indicate statistical significance in comparison with OECC and Diazepam (*p<0.05; **p<0.01; ***p<0.001; ****p<0.0001 vs. Control; #p< 0.05; ###p<0.001 vs Petrosamine or DZP).

Inhibitory Avoidance Test

The inhibitory avoidance task caused by electroshock indicated that all tested doses of petrosamine retained the zebrafish memory in the test session (*p<0.05, ***p<0.001, ****p<0.0001 vs Training), especially at the dose of 4 mg/kg that best retained the zebrafish memory when compared to the reference standard drug (DNZP - donepezil, *p<0.05), unlike the control group treated with DMSO that had impaired memory retention, since the latency times to enter the dark compartment between the training session and the test session did not differ (Figure 5).

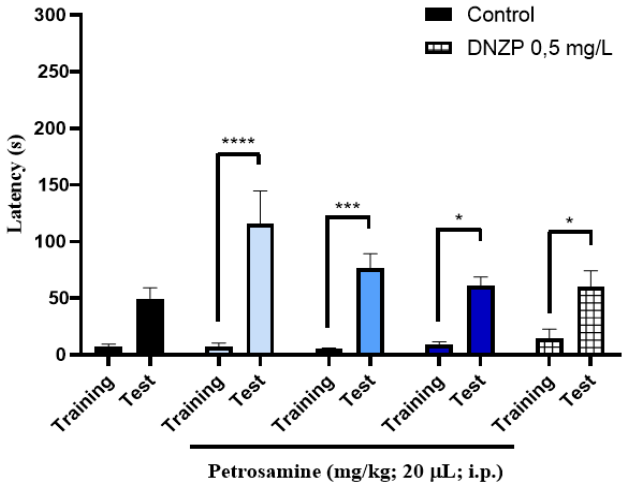


Figure 5. Effect of pretreatment with petrosamine on the memory retention index of adult zebrafish in the Inhibitory Avoidance Test (0–5 min). Grupo controle (DMSO a 3%); DNZP – Donepezil (0,5 mg/L; 20 µL; i.p.). Values represent the mean ± standard error of the mean for 6 animals/group; Two-way ANOVA followed by Tukey's test (*p<0.05, ***p<0.001, ****p<0.0001 vs. Training).

In addition, the retention index indicated a significant difference between the petrosamine and DNZP groups ($^{\#}p<0.05$ vs DNZP), showing that the group treated with petrosamine (4mg/kg) better preserved the fish's memory of the aversive stimulus ($p<0.05$) (Figure 6).

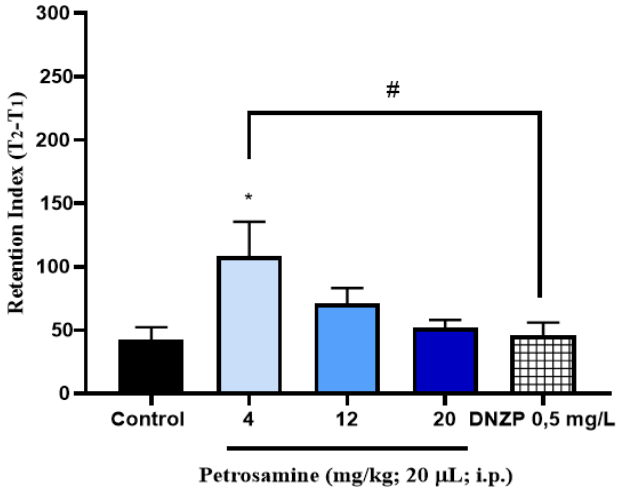


Figure 6. Effect of pretreatment with petrosamine on the memory retention index of adult zebrafish in the Inhibitory Avoidance Test (0–5 min). Grupo controle (DMSO a 3%); DNZP – Donepezil (0,5 mg/L; 20 µL; i.p.). Values represent the mean ± standard error of the mean for 6 animals/group; One-way ANOVA followed by Tukey's test ($^{\#}p<0.05$ vs DNZP*)*.

The evaluation of the effect of ethanol on memory acquisition in zebrafish was also investigated. Petrosamine at the lowest effective dose (4mg/kg) significantly preserved (****$p<0.001$ vs Training) memory and protected ($^{\#}p<0.05$ vs Ethanol) the fish from the deleterious effect of alcohol on memory (Figure 7).

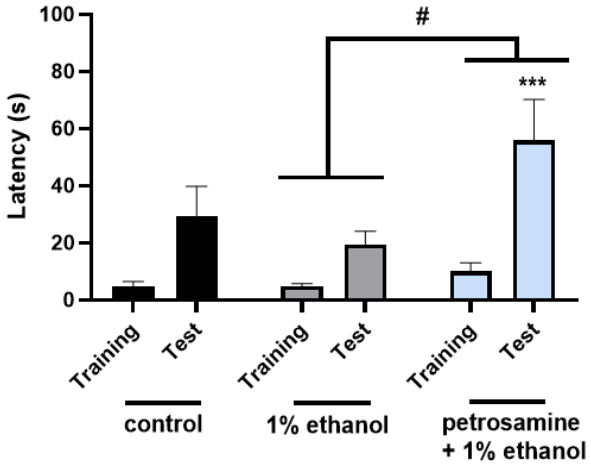


Figure 7. Effect of pretreatment with petrosamine on memory in adult zebrafish after exposure to ethanol 1% (0-20 min). Values represent the mean ± standard error of the mean for 6 animals/group; Two-way ANOVA followed by Tukey's test ($^{\#}p<0.05$ vs. EtOH 1%).

According to the graph, the retention index indicated a difference between the petrosamine (4mg/kg) group and 1% EtOH ($^{\#}p<0.05$ vs EtOH), showing that the group treated with petrosamine (4mg/kg) protected the fish's memory from the damaging effect of alcohol (Figure 8).

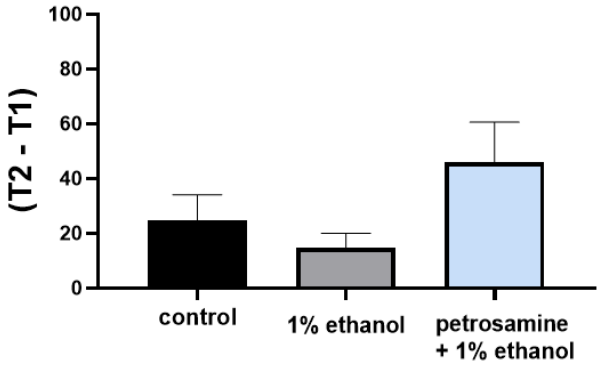


Figure 8. Effect of pretreatment with petrosamine on memory retention index in adult zebrafish after exposure to ethanol 1% (0-20 min). Values represent the mean ± standard error of the mean for 6 animals/group; One-way ANOVA followed by Tukey's test ($^{\#}p<0.05$ vs EtOH).

Molecular docking analysis

Docking of the anxiolytic effect on the GABAergic system

To estimate the theoretical anxiety mechanism of petrosamine, the potential modulation of the ligand on $GABA_AR$ receptors was analyzed (Figure 9). At the end of the simulations, an RMSD in the order of 1.97 Å was found for petrosamine, which expresses a low root mean square deviation of the pose of the ligand fitting into the binding site on the receptor (Table 1). The ligand complexed to the receptor in the same DZP agonist binding site, located between the C and D chains in the extracellular domain (Figure 9a) with a calculated affinity energy order of -8.82 kcal/mol (Table 1). This energy range indicates that petrosamine shows optimum specificity for the $GABA_AR$ receptor, while DZP showed an affinity energy value of -7.16 kcal/mol (Table 1). This analysis suggests that petrosamine formed an energetically more favorable ligand-$GABA_AR$ complex than DZP, indicating that the ligand is an ideal candidate to act as a $GABA_AR$ receptor agonist.

In relation to the interactions that the ligand formed with the residues of the docking site, it was possible to observe that petrosamine formed hydrophobic interactions in common with DZP in relation to the aromatic side chain of the Tyr58 and Phe77 residues[46], both through their halogen-substituted aromatic structures (Figure 9b). Here, it is worth noting that petrosamine showed a parallel-oriented π-stacking interaction with the aromatic center of Tyr58, with a distance of 3.98 Å from its bromo-substituted aromatic ring (Figure 9b), while the H-bond acceptor carbonyl interacted with the positively charged amine portion (HN^+) of the His102 residue (3.60 Å), where the ligand-protein distance calculated in Å expresses a weak H-bond interaction (Table 1). These analyses suggest that petrosamine may act on $GABA_AR$ receptors in a similar way to DZP.

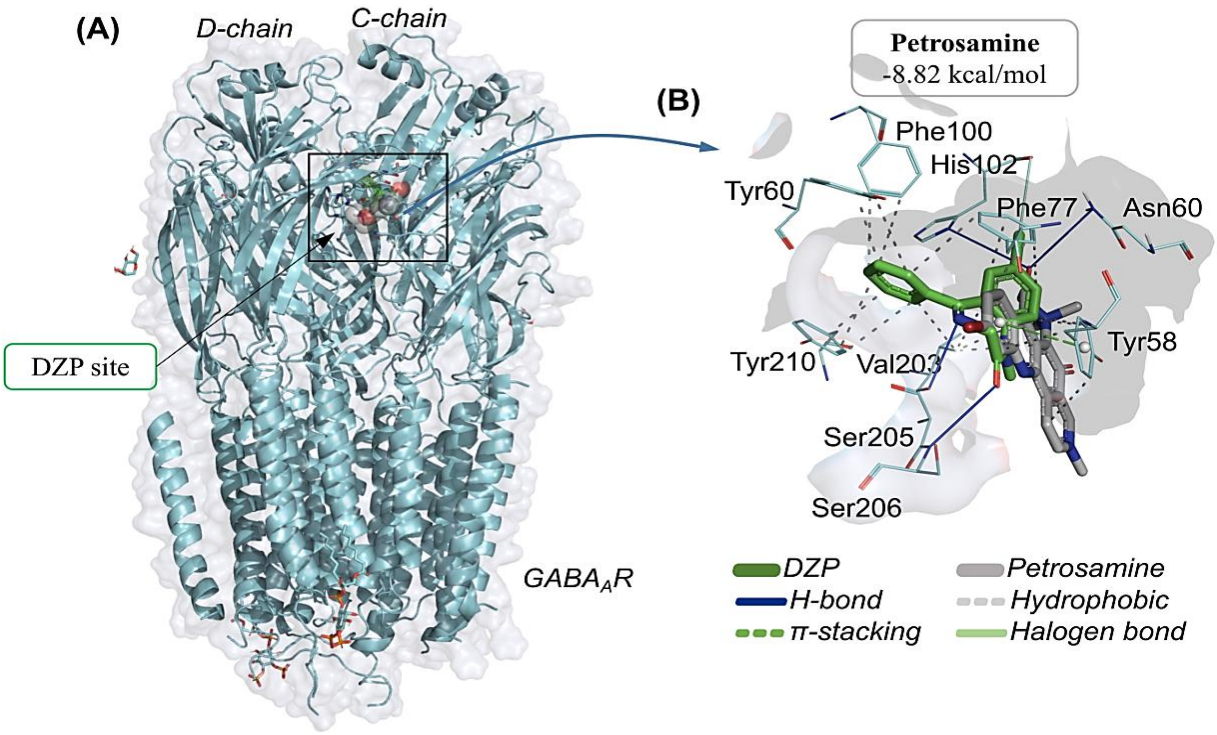


Figure 9. (a) Three-dimensional visualization of the coupling of the ligand petrosamine (grey color) and DZP (green color) in the $GABA_AR$ receptor (cyan color) and (b) three-dimensional visualization of the ligand-protein interactions between the ligands petrosamine (yellow color) the amino acid residues of the $GABA_AR$ binding site (cyan color color).

Table 1

Data from molecular docking simulations between the petrosamine ligand and the CAII and $GABA_AR$ targets expressed in RMSD and affinity energy, and details of the ligand-protein interactions expressed in type of interaction, amino acid residue, chain and distance of interactions.

Target	Ligand	RMSD	Affinity energy (kcal/mol)	Interactions			
				Type	Residue	Chain	Distance (Å)
CAII	Petrosamina	1.05	-6.84	Hydrophobic	Ile91	A	3.42
					Gln92	A	3.58
				H-bond	Gln92	A	2.20
					Thr200	A	3.27
	TE1*	1.89	-5.02	Hydrophobic	Ile91	A	3.66
					Gln92	A	3.60
				H-bond	Arg58	A	3.34
					Asn67	A	1.44
					Gln92	A	2.35
				Water bridges	Asn62	A	3.35
					Glu69	A	3.14

				π-Stacking	Phe131	A	4.76
$GABA_AR$	Petrosamina	1.97	-8.82	Hydrophobic	Tyr58	C	4.57
					Tyr58	C	4.23
					Tyr58	C	4.57
					Phe77	C	3.56
					Val203	D	3.67
				H-bond	Asn60	C	3.71
					His102	D	3.60
				π-Stacking	Tyr58	C	3.98
	DZP*	1.72	-7.16	Hydrophobic	Tyr58	C	3.52
					Phe77	C	3.47
					Phe100	D	3.83
					Phe100	D	3.92
					Tyr160	D	3.56
					Val203	D	3.95
					Tyr210	D	3.38
					Tyr210	D	3.86
				H-bond	Ser205	D	2.94
					Ser206	D	3.16
				Halogen bond	His102	D	3.82

*control ligand used in molecular docking simulations to compare ligand-protein interaction.

Docking of the anticonvulsant effect

In order to evaluate the theoretical mechanism of anticonvulsant action of petrosamine, the binding potential to the CAII enzyme was analyzed (Figure 10). At the end of the cycle of independent simulations, it was possible to observe that the ligand complexed with the enzyme in the same binding site as the inhibitor TE1 (Figure 10a), with an RMSD deviation of around 1.05 Å (Table 1), indicating that the simulations performed within an ideal statistical threshold that allows the simulation model to be reproduced[92]. The formation of the petrosamine-CAII complex showed a calculated affinity energy value of -6.84 kcal/mol (Table 1), indicating that the ligand has an optimal target specificity profile (optimal < -6.0 kcal/mol)[93].

With regard to ligand-protein interactions, it was possible to observe that petrosamine formed hydrophobic interactions in common with the co-crystallized inhibitor TE1 in relation to the alkyl side chain of the Ile91 and Gln92 residues (Figure 10b), with a strong contribution from its bromo-substituted aromatic ring (A ring), while the carbonyl group of the heterocyclic structure (D ring) interacted with the polar portion of the Gln92 residue (2.20 Å), where the ligand-protein distance (expressed in Å) characterizes a strong H-bond interaction (Table 1)[92]. Although has shown interactions in common with the inhibitor, the docking pose of petrosamine means that the ligand does

not form interactions with key residues of the enzyme's active site, which include Asn67 and Phe131, which characterize regions of strong H-bond interaction and π-stacking interaction, respectively[94].

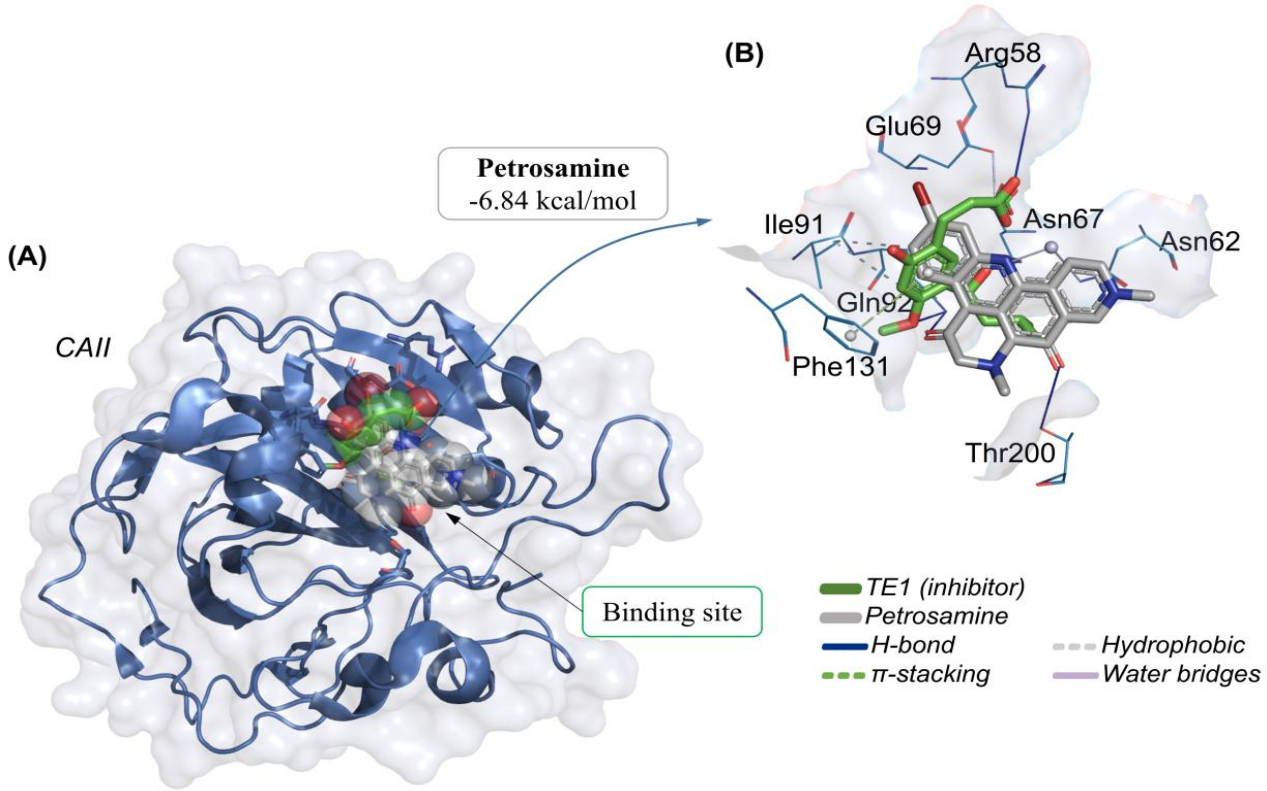


Figure 10. (a) Three-dimensional visualization of the coupling of the ligand petrosamine (grey color) and the inhibitor TE1 (green color) in the CAII protein (blue color) and (b) three-dimensional visualization of the ligand-protein interactions between the ligands petrosamine (yellow color) and TE1 (green color) and the amino acid residues of the CAII active site (blue color).

Docking inhibitor AChE

The molecular docking studies show the projection of interactions formed between the ligands when associated with the target receptor, resulting in the formation of a complex through the affinity character; the molecular docking simulations showed the best affinity profiles for each compound, where Figure 11 (A) shows both complexes estimated in the research, where GNT (orange) has an energy value equal to -7.2 kcal/mol and a variation equal to 1.820 Å (RSMD); the petrosamine compound showed a more intense energy value equal to -9.3 kcal/mol, while the RMSD variation was equal to 1.998 Å.

Analyses of the molecular docking simulations show in Figure 11 (B) all the interactions formed between the GNT compound associated with the cavity of the catalytic site; among the interactions were formed with six amino acid residues distributed in seven hydrophobic interactions with five amino acid residues Trp86 (3.85 Å, 3.59 Å and 3.81 Å), Tyr124 (3.78 Å), Phe297 (3.98 Å) Tyr337 (3.99 Å) and Phe338 (3.85 Å) and only one hydrogen bond with Ser203, with a value equal to 2.89 Å. The data shows that the amino acid residues involved in the interactions are classified as relevant residues in the potential determination of the inhibitory effect of anti-acetylcholinesterase activity,

serving as a basis for the determination of viable compounds through virtual screening studies. With regard to the petrosamine compound, Figure 11 (C) shows all the interaction relationships formed between the ligand when associated with the target interaction cavity. The results show that the ligand exerted only three hydrophobic interactions through the residues Trp286 (3.96 Å and 3.69 Å) and Tyr341 (3.41 Å); a Pi-staking style interaction through the bond with the Trp286 amino acid residue with a distance value of 3.64 Å and, finally, the relationship between the ligand and the protein resulted in the formation of only one salt bridges style interaction with the Glu292 residue; all the other values referring to the distance values duly associated with the types of interactions are shown in Table 2.

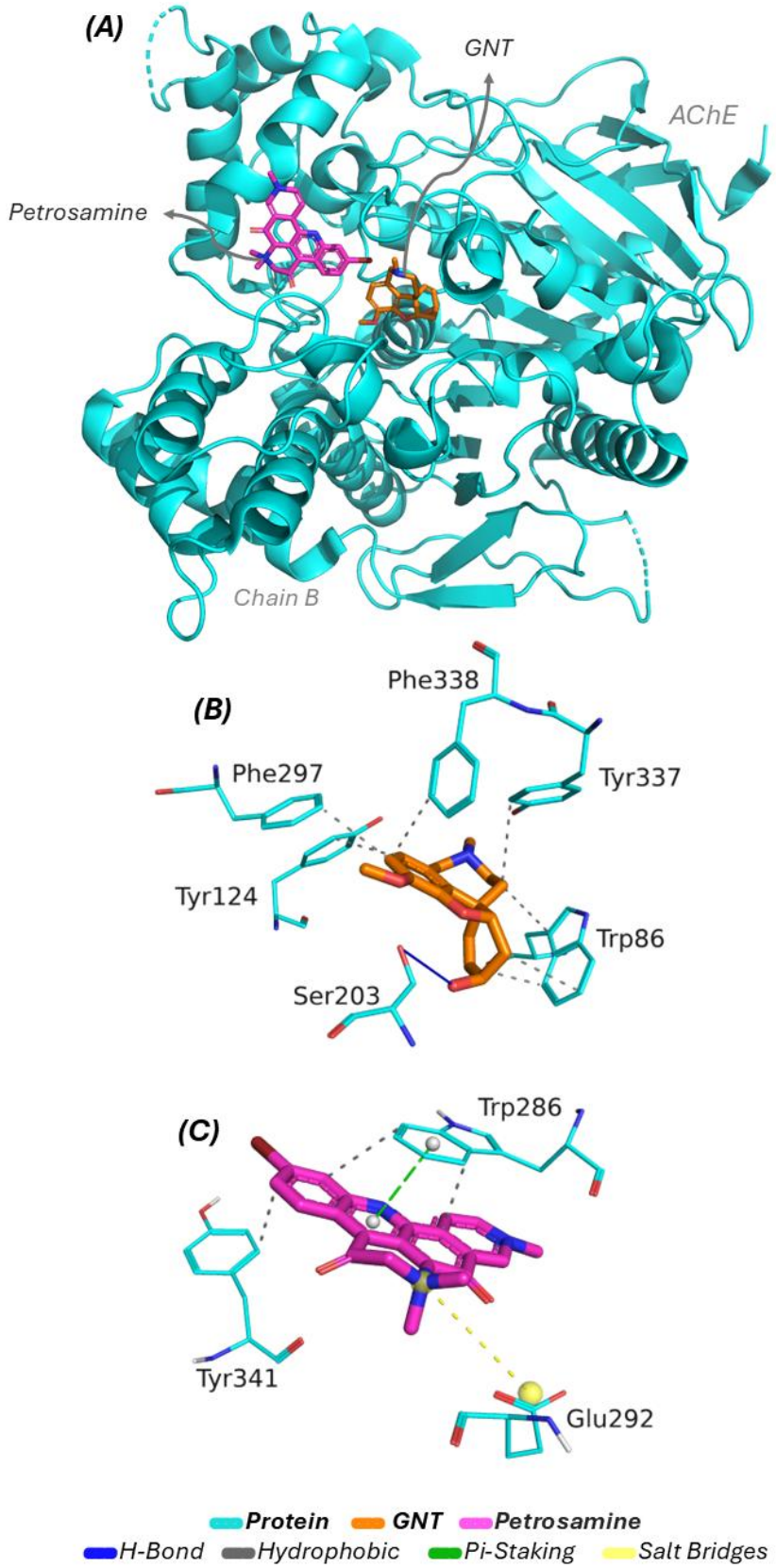


Figure 11. Molecular docking simulations of the AChE system. (A) overview of the complexes formed (B) interactions formed between the crystallised inhibitor GNT (C) projection of the interactions formed between the petrosamine compound associated with amino acid residues.

According to the molecular docking simulations, the data showed that both the GNT and petrosamine compounds exerted affinity on different portions of the target receptor, resulting in

different affinity profiles, with a partial absence of competition for the same site. In view of the data on the interactions formed, it is clear that the compounds evaluated showed different interactions, due to the projection of the interactions predicted in the affinity studies. These results indicate that the potential therapeutic effect linked to the compound petrosamine is not associated with the crystallised inhibitor site, so there is no competitive effect, resulting in its possible use through a synergistic effect.

Table 2. Values linked to interactions via AChE.

Complex	Energy (kcal/mol)	Interaction Type	Residue (Distance in Å)
GNT/AChE	-7.2	Hydrophobic	Trp86 (3.48, 3.59 e 3.66), Tyr124 (3.95), Phe297 (3.65) e Phe338 (3.88)
		H-Bond	Ser203 (2.99) e Tyr337 (2.07)
Petrosamine/AChE	-9.3	Hydrophobic	Trp286(3.96 e 3.69) e Tyr341 (3.41)
		Pi-Staking	Trp286(3.64)
		Salt Bridges	Glu292 (5.01)

MPO-based ADME study

MLP analysis and druglikeness

A multi-parameter optimization (MPO) model developed by Pfizer, Inc. is capable of estimating the pharmacokinetic profile of small molecules with properties convenient to the CNS. According to Wager et al. (2016)[95], weak bases with low lipophilicity (logP ≤ 3) and which are larger and more polar (TPSA 40-90 Å²) than compounds commonly active in the CNS show an alignment between safety and *in vitro* properties of ADME: high apparent permeability (P_{app} > 10×10-⁶ cm/s), low passive efflux by P-gp and low clearance of the intrinsic fraction in plasma ($CL_{int,u}$ < 8.0 mL/min/kg)[96]. These attributes are related to the oral absorption and metabolic stability of drugs[97].

A topological analysis of the molecular lipophilicity potential (MLP) can provide relationships between the lipophilic surface and polar surface of small molecules with their permeability and diffusion potential in the cellular lipid bilayer[98]. In this analysis, it was possible to observe that the aromatic and heteroaromatic rings of petrosamine have a moderately liposoluble molecular surface (green color spectra in Figure 12a), where the calculated lipophilicity (logP) in the order of 2.04 is the result of the electron-withdrawing inductive effect of the bromo-phenyl group (blue color spectra in Figure 12a), which showed a high MLP contribution index (0.44). In the CNS MPO desirability radar, it was possible to observe that the intrinsic lipophilicity indices (logP) and at physiological pH (logD at pH 7.4) are within the ideal spectrum of druglikeness that follow safety trends and ADME properties, when aligned with the MW and TPSA attributes (Figure 12b), resulting in an MPO score in the order of 5.5 (on a scale ranging from 0 to 6) (Table 3).

Table 3. Physicochemical properties of petrosamine calculated and applied to Pfizer, Inc., scoring criteria, which include CNS MPO score, Pfizer rule, and Golden Triangle rule.

Property	Value	T^0
ClogP	2.04	1.00
$ClogD_{7.4}$	2.16	1.00
MW	423.28 g/mol	0.55
TPSA	51.96 Å²	1.00
HBD	0	1.00
pKa	4.63 (basic)	1.00
CNS MPO score	5.5	
Pfizer rule	Accepted	
Golden Triangle rule	Accepted	

Drug space and pharmacokinetic properties

The physicochemical attributes of lipophilicity, molecular size and polarity were aligned to assess the oral absorption profile and CNS activity of petrosamine. From logP < 3, it was possible to observe that the compound resides within a physicochemical space formed by drug candidates active in the CNS (Figure 12c) with a high degree of safety and a favorable ADME profile (TPSA > 40 Å²), especially due to the calculated polar surface area of 51.96 Å², with a strong structural contribution from the polar surface of the carbonyl groups (C=O), whose calculated areas were equal to 17.07 Å²[99]. This empirical analysis corroborates the descriptor of access to the CNS by permeability in the blood-brain barrier (logBB) in the order of -1.99, indicating a gradual action in the brain (Table 4), attributed to the balance between lipophilicity and polarity, where the estimated VD of 1.93 L/kg indicates that petrosamine can be widely distributed in biological tissues (Table 4).

When the lipophilicity of the protic species, calculated at 2.16 for the chemical species distributed at pH 7.4, was aligned with the molecular size calculated within the range of MW < 450 g/mol (Figure 12d), it was possible to note that petrosamine resides in a physicochemical space formed by compounds with high P_{app} MDCK and low $CL_{int,u}$, whose ranges are satisfied by the Golden Triangle rule (-2< logD ≤ 5 and 200 g/mol < MW ≤ 500 g/mol)[61]. This result corroborates the pharmacokinetic descriptors predicted by the ADME consensus test, where the estimated P_{app} MDCK of 2.8×10^{-5} cm/s is indicative of high cell permeability which, when aligned with the low clearance assessed by $CL_{int,u}$ = 4.29 mL/min/kg, guarantees good intestinal absorption. However, the charged nature of petrosamine may reduce the oral bioavailability of the compound ($_{F<50\%}$ descriptor), since positively charged compounds can be P-gp substrates (Table 4)[100].

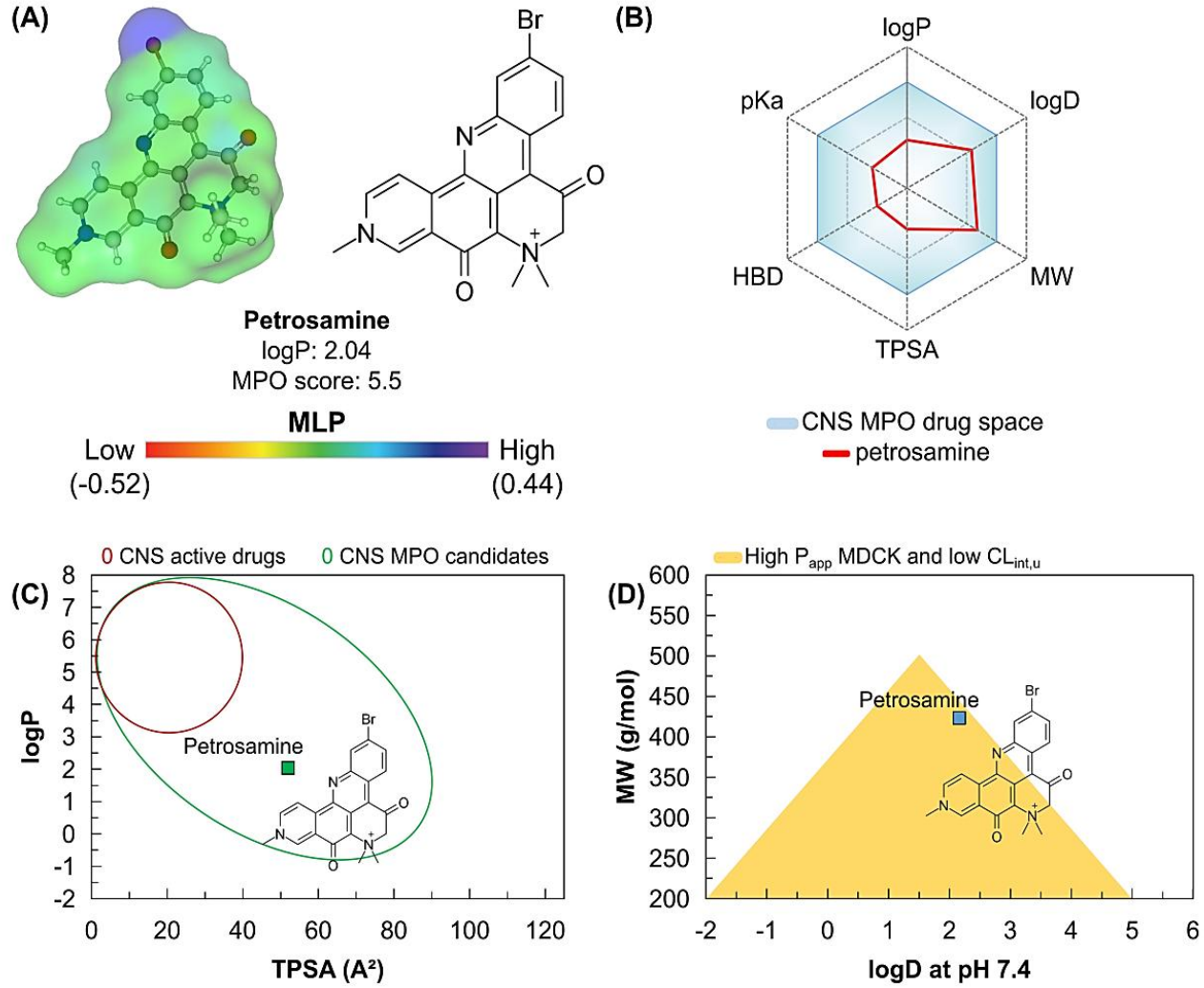


Figure 12. (a) topological analysis of molecular lipophilicity potential (MLP), (b) druglikeness radar resulting from the CNS MPO test, (c) alignment between lipophilicity (logP) and polarity (TPSA) in estimating the access to the CNS and (d) alignment between lipophilicity at physiological pH (logD at pH 7.4) and molecular weight (MW) in estimating the oral absorption profile and metabolic stability.

Table 4. Pharmacokinetic properties of petrosamine predicted by consensus ADME testing between the ADMETlab 3.0, Deep-PK and ProTox-II platforms.

Property	**Value**	**Source**
P_{app} MDCK	$2.8x10^{-5}$ cm/s	ADMETlab 3.0
P-gp substrate	Substrate	ADMETlab 3.0
$F_{<50\%}$	1.00	ADMETlab 3.0
VD	1.93 L/kg	ADMETlab 3.0
PPB	61.13%	Deep-PK

logBB	-1.99	Deep-PK
BBB	Penetrable (High Confidence)	Deep-PK
$CL_{int,u}$	4.29 mL/min/kg	ADMETlab 3.0
Mutagen	– (0.62)	ProTox 3.0
DILI	– (0.63)	ProTox 3.0

Site of metabolism prediction

Prediction of the phase I metabolism site allows us to estimate the secondary metabolites formed in human liver microsomes (HLM), defining the metabolic profile of drug candidates and the toxic effect of these processes[101]. The commonly known biotransformations of the CYP450 isoform system are based on oxidation, reduction and deacylation reactions of polar N- and O- centers, as well as oxygenation and hydrogenation reactions in aromatic centers, constituting more polar metabolites for excretion[102]. However, some metabolites can be reactive and bind covalently to unwanted targets such as proteins and DNA, resulting in liver damage[103].

In this predictive test, it was possible to observe that petrosamine has alkyl groups based on N-CH_3 which are susceptible to demethylation, forming secondary metabolites based on N-dealkyl-petrosamine, mostly by CYP450 isoforms type 2C9, 2D6 and 3A4 in phase I metabolism (Figure 13). These reactions were characterized as stable N-dealkylation reactions, indicating that the metabolites formed have low reactivity and, by extension, low toxic response by metabolic activation, corroborating the low probability of the compound inducing liver damage (DILI descriptor) and mutagenicity (Table 4).

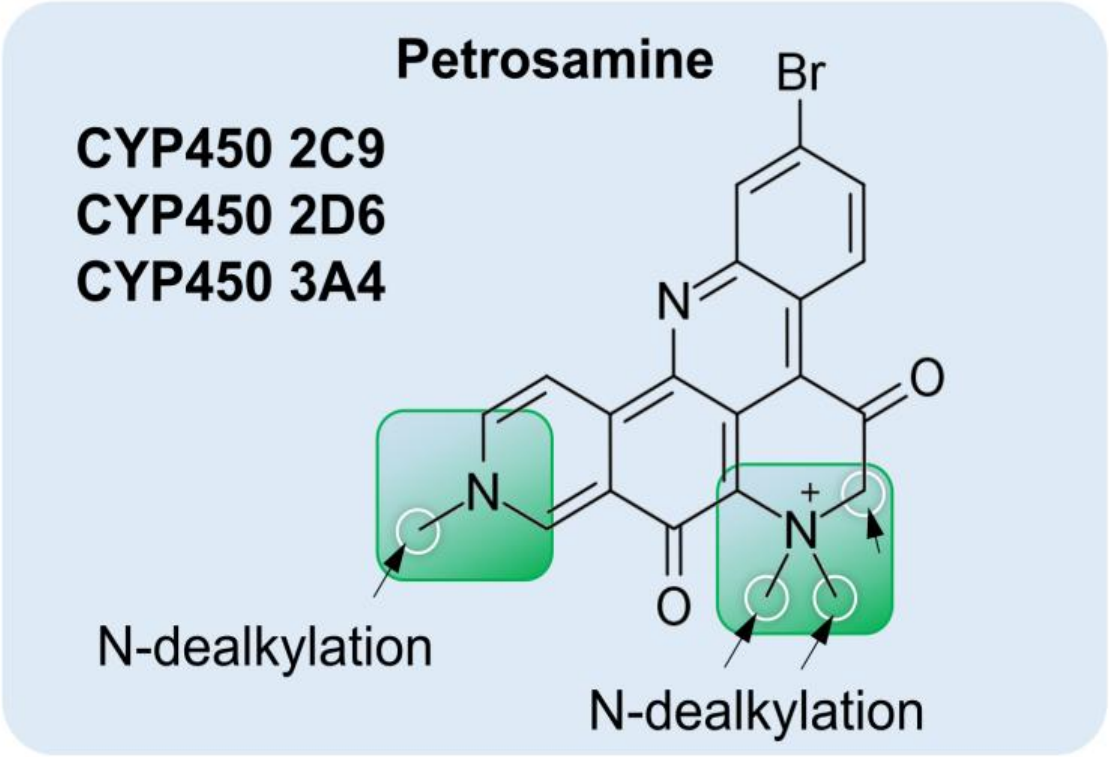


Figure 13. Two-dimensional map of petrosamine metabolism site prediction, with reactions based on N-dealkylation dependent on CYP450 2C9, 2D6 and 3A4 isoforms.

Quantum Chemical Calculations

Chemical reactivity

The energy values of the highest occupied molecular orbital (HOMO) and the lowest unoccupied molecular orbital (LUMO), as well as their energy gap, directly affect the chemical reactivity of the molecule. The HOMO-LUMO energy gap represents the energy required to promote an electron between these two levels. This energy "gap" is crucial for predicting a molecule's reactivity, its ability to absorb light, and its electronic and optical properties. A smaller gap generally indicates a more reactive and less stable molecule while a larger gap indicates the opposite. DFT calculations resulted in Ionization Energy (I), Electron Affinity (A), and Energy Difference (GAP) values of -10.275 eV, -4.627 eV, and 5.648 eV, respectively. Figure 14 shows, in addition to these values, an overview of all occupied and virtual molecular orbitals of petrosamine and the geometric shape of the HOMO and LUMO frontier orbitals.

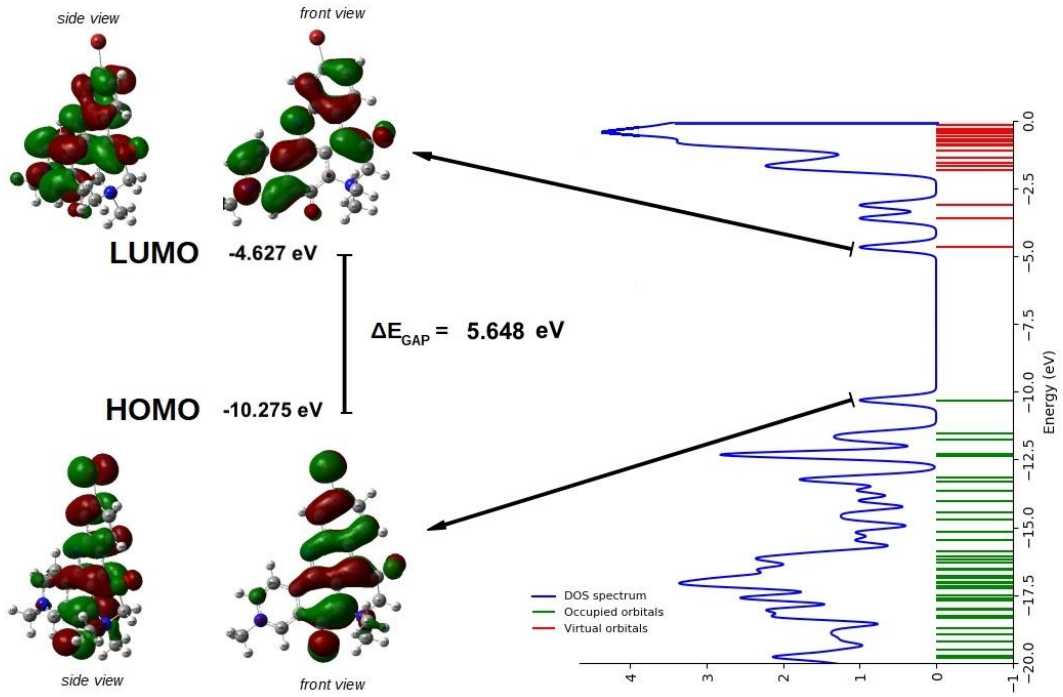
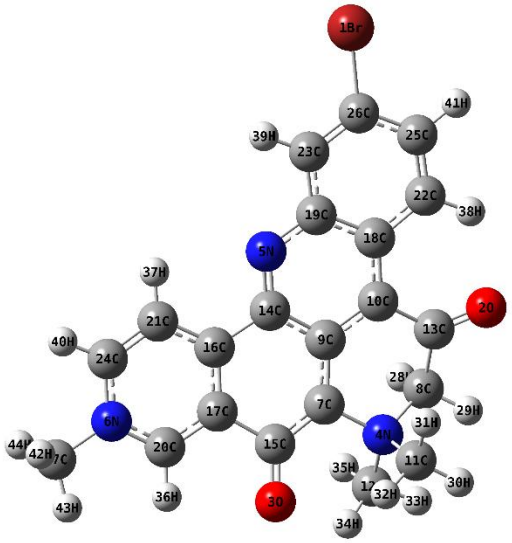


Figure 14. Petrosamine molecular orbitals, frontier orbitals energy, and energy HOMO - LUMO gap.

Electronegativity represents a general tendency of a molecule to move towards regions with high electron density. Due to its calculated electronegativity of 7.451 eV, petrosamine likely appears to be susceptible to nucleophilic attacks at suitable sites. Chemical hardness and softness are related to deformations of the electron cloud under external fields or during charge transfer. In practical terms, high hardness is associated with low polarizability and weak density responses, while high softness implies greater polarizability and more pronounced distortions in the electron cloud[112]. Numerically, one is the inverse of the other, as shown in equations 6 and 7. The calculated hardness and softness values for petrosamine were 2.824 eV and 0.354 eV, respectively. Furthermore, the electrophilicity parameter, which measured the susceptibility of the compound to accept electrons, was 9.830 eV.

As indicated in equations 13 to 15, the indices f^+, f^- and f^0 were calculated by approximating them with the Hirshfeld charges on each atom in order to obtain their gereral susceptibility to a chemical reaction. Subsequently, Δf parameter, which is calculated using the expression [$\Delta f = f^+ - f^-$], were used to evaluate the sites that are most prone to nucleophilic or eletrophilic attack. The results are summarized in Table 5.

Table 5. Fukui condensate for the petrosamine.

Petrosamine	Atoms	Δf	Atoms	Δf
	**1Br**	**-0.036691**	23C	-0.000765
	2O	0.011838	24C	0.018971
	3O	**-0.086285**	25C	0.025296
	4N	-0.000334	26C	-0.024195
	5N	**0.037491**	27C	0.009387
	6N	**0.035595**	28H	-0.000451
	7C	**-0.080256**	29H	-0.001471
	8C	-0.000923	30H	-0.005486
	9C	-0.007249	31H	-0.005540
	10C	-0.011725	32H	-0.000924
	1 C	-0.004921	33H	-0.005360
	12C	-0.003943	34H	-0.003872
	13C	0.017073	35H	-0.004228
	14C	-0.006129	36H	0.009384
	15C	**-0.046336**	37H	0.008975
	16C	**0.047635**	38H	-0.001804
	17C	**0.031745**	39H	-0.000575
	18C	0.020790	40H	0.010486
	19C	-0.006255	41H	0.002837
	20C	0.030129	42H	0.009606
	21C	0.016616	43H	0.008636
	22C	-0.017071	44H	0.010357

These results highlight that the atoms with greatest electrophilic character, and therefore with greatest propensity to carry out eletrophilic attack, are, in order of magnitude 16C > 5N > 6N > 17C. Otherwise, the most prone atoms to nucleophilic attack in petrosamine are 3O > 7C > 15C > 1Br.

Molecular electrostatic potential (MEP)

Molecular electrostatic potential (MEP) maps the charge distribution around a molecule, indicating regions prone to electrophilic or nucleophilic interactions; its surfaces aid in predicting reactivity, molecular recognition, and binding sites in chemical and biochemical studies. In this type of representation, regions with lower electron density appear blue, while regions rich in electrons appear red with the scale varing from red to blue from -0.24 to 0.24 eV. Figure 15 shows the electrostatic potential of petrosamine in its native form. In it, we can observe that the tones approach blue. This was expected, since petrosamine in its native form has tetravalent nitrogen (4N), that is, a positive charge, which induces this electronic deficiency in the molecule. The regions with the greatest electron deficiency (blue colored), and consequently the most susceptible to nucleophilic attacks, are those around the nitrogen atoms

(4N, 5N, and 6N), given that this element can withstand positive charges well. On the other hand, the regions most susceptible to electrophilic attacks are those with higher electron density, which are associated, as illustrated in Figure 15, with a color close to red. Thus we can identify that the regions close to the bromine atom (1Br) and the oxygen atoms (2O and 3O) have this characteristic. However, based on the density scale, we cannot say that these regions have a high charge concentration, leading us to believe that the molecule likely reacts from its electrophilic sites (blue colored).

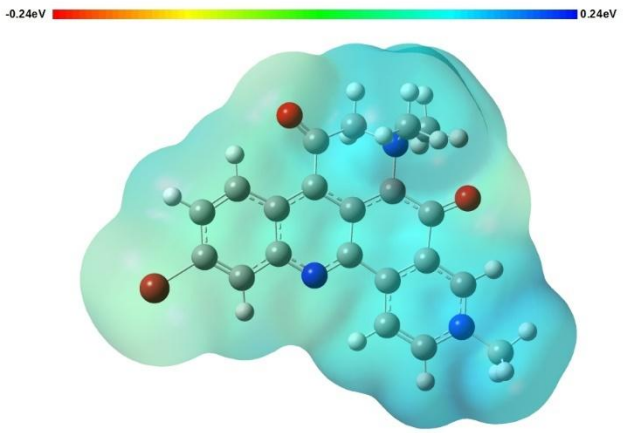


Figure 15. Electrostatic potential map of petrosamine.

Discussion

In this study, we aimed to carry out a comprehensive analysis of the neuroprotective potential of the pyridoacridine alkaloid petrosamine of strictly marine origin, derived from sessile marine invertebrates, and its properties involving acute toxicity and behavioral tests in different aspects, such as anxiety, environmental exploration, convulsion, learning and memory, using adult *zebrafish* as an animal model.

Evaluating the toxicity of petrosamine in in vivo models is unprecedented, as no published study with the marine alkaloid has evaluated toxicity in an animal model. A study carried out by Marshall and collaborators[36] showed that three marine pyridoacridine molecules, namely deoxyamphimedine, neoamphimedine and amphimedine, which have the same carbon skeleton as petrosamine, isolated from sponges of the genus *Xestospongia* collected in the Philippines, showed affinity for DNA with notable cytotoxic activity *in vitro* models. Although these

compounds are very similar in chemical terms, the data show that their small structural differences significantly alter their biological activities[104].

In the evaluation of neurobehavioral symptoms, apathy, anxiety, and irritability are the first neuropsychiatric symptoms associated with neurodegenerative diseases[105]. The evaluation of the anxiolytic and anticonvulsant effects of petrosamine was examined using the adult zebrafish model, marking the first report in the scientific literature. The open field test serves as a behavioral parameter used to evaluate the action of drugs that may affect the central nervous system of the adult zebrafish, taking into consideration the swimming activity of the animal, as well as its movement to analyze whether there was a restriction of locomotion, resulting in a more static animal or if the swimming continues with the regular pattern[61,62].

The lower doses of petrosamine, despite reducing the swimming of zebrafish in the open field test, did not cause the sedative effect observed in the Diazepam group. The evaluation of anxiety can be observed in experimental animal models, representing a natural emotional response to potentially threatening situations, such as exposure to novelty, predator odor, or other threatening contexts[66,67,68]. The zebrafish is increasingly used in translational studies of stress and anxiety, as well as in screening drugs in the central nervous system (CNS)[69,70], since it has a high genetic homology with humans[71], and exhibits robust anxiety-like behaviors[72,73], which are highly sensitive to various genetic[67], epigenetic[74,75,76], neuropharmacological[77], and environmental[78,79,80] factors. The higher doses of petrosamine caused anxiolytic behavior in the light and dark tests. When correlating the results of the OFT and ODT, it was observed that the dose of 12 mg/kg caused anxiolytic behavior without sedation in the animals.

The GABAergic system is the main action pathway of anxiolytic medications produced from natural products[81,82]. Flumazenil is used in the clinic to block the sedative and hypnotic effects caused by benzodiazepine overdoses via GABAergic neurotransmission. Therefore, it can be used in the investigation of the mechanism of action of new compounds with anxiolytic effects through the same action pathway as Diazepam. The pre-treatment with flumazenil blocked the anxiolytic effect of petrosamine, indicating that the anxiolytic action of petrosamine occurs in the same interaction region as Diazepam in the GABAA receptor. These indications were confirmed by *in silico* studies, which showed petrosamine binding to the active binding site of Diazepam on the $GABA_A$ receptor, suggesting that petrosamine formed a ligand-$GABA_{AR}$ complex that was energetically more favorable than Diazepam, making it an ideal candidate to act as an agonist of the GABAAR receptor. Regarding the interactions, it was possible to observe that petrosamine formed hydrophobic interactions in common with Diazepam concerning the aromatic side chain of the residues Tyr58 and Phe77[46], both through

their halogen-substituted aromatic structures. Additionally, petrosamine showed a π-stacking interaction oriented parallel to the aromatic center of Tyr58, while the carbonyl hydrogen bond acceptor interacted with the positively charged amine portion (HN^+) of the His102 residue. These analyses suggest that petrosamine may act on the GABAA receptor in a manner similar to Diazepam.

One of the most commonly used approaches to induce seizures in animals is chemoconvulsants, such as pentylenetetrazole (PTZ)[86,89]. When administered PTZ, the zebrafish progresses through a distinct set of movements and postures that culminate in generalized tonic-clonic seizures[87,88]. Studies indicate that PTZ induces seizures mainly through binding to the gamma-aminobutyric acid (GABAA) receptor, preventing the neuroinhibitory action of GABA[87,88]. Petrosamine, in addition to causing anxiolytic behavior through GABAergic modulation, delayed the convulsive behavior in stages I, II, and III induced by PTZ. Molecular docking studies indicated that the effect of petrosamine in causing anticonvulsant behavior may be related to its complexation with the enzyme CAII at the same binding site as the inhibitor TE1, with an RMSD deviation of about 1.05 Å. The formation of the petrosamine-CAII complex showed a calculated binding energy value of -6.84 kcal/mol, indicating that the ligand has an optimal target specificity profile (optimal < -6.0 kcal/mol)[91].

In the investigation of anti-Alzheimer's therapeutic agents, some studies report the potential of petrosamine as a neuroprotective agent[7,22,33,106]. Petrosamine is an alkaloid derived from two amino acids, tryptophan and tyrosine, which shows strong AChE inhibitory activity[7]. The pentacyclic alkaloid petrosamine has neuroprotective activity with an inhibitory action against the AChE enzyme about six times greater than the potency of galantamine, an AChE inhibitor currently used in the treatment of Alzheimer's disease[20]. To evaluate the effect of petrosamine on memory, we conducted the inhibitory avoidance test induced by electroshock in adult zebrafish. The effect on memory was dose-dependent, with lower doses of petrosamine increasing memory preservation as observed by the retention index. Furthermore, we observed that the lowest dose of petrosamine prevented the deleterious effects of alcohol on the memory of adult zebrafish after acute exposure. This neuroprotective activity is associated with the quaternary ammonium group of the alkaloid's D ring, which is responsible for the catalytic site interactions between petrosamine and AChE[7,21].

A relevant aspect observed by Ribeiro et al. (2024)[33] refers to the change in AChE activity after aluminum-induced neurotoxicity *in vivo*. *Zebrafish* embryos subjected to 50 μM $AlCl_3$ had AChE activity increased by 67%. Petrosamine led to a 92% decrease in AChE activity, showing high inhibition of AChE by this natural product.

In silico tests carried out by Nukoolkarn[20] and collaborators and Gartshore[22] and collaborators defined the contact points in the active site of the AChE enzyme that can select the design of new AChE inhibitors based on the molecular skeleton of the bioactive compound as observed with the natural marine alkaloid petrosamine and which are in agreement with the in silico results obtained in this research.

As can be seen, knowledge of the biological effects of pyridoacridines and numerous analogues is essential for a better understanding of the pharmacological properties of marine bioactives. These studies show that only evaluating the *in vitro* activity of isolated alkaloids is insufficient, given that other aspects, mainly pharmacokinetic and toxicity, are related to the clinical potential of bioactive molecules. Therefore, studies aimed at evaluating these promising alkaloids in cell cultures and *in vivo* models are indispensable. All these efforts should culminate in the identification of good structures and the subsequent development of more effective and safer anticholinesterase drugs[21].

The HOMO-LUMO energy gap of petrosamine suggests intermediate chemical reactivity and moderate kinetic stability, consistent with the established correlation between smaller gap and greater molecular reactivity. The electronegativity value obtained reflects the capacity to accept electron density, rendering the species susceptible to nucleophilic attacks at appropriate electrophilic sites. The high chemical hardness indicates low polarizability and limited electronic response to external perturbations, while the corresponding softness is associated with electron cloud deformability, corroborating the intermediate reactivity profile. The high electrophilicity index confirms the tendency to accept electrons, a relevant property for rationalizing interactions with nucleophiles in different chemical environments. Molecular electrostatic potential (MEP) analysis reveals predominantly blue regions around the cationic nitrogens and reddish tones near the O/Br atoms, in agreement with Fukui indices, demonstrating the convergence between these approaches in identifying local reactive sites.

Conclusion

This study determined the pharmacological activity of the alkaloid petrosamine extracted from the marine sponge species *Petrosia* sp., being one of the first to investigate the anxiolytic, anticonvulsant, and memory-preserving effects in adult zebrafish. The results show that petrosamine was not toxic, with potential anxiolytic effects, anticonvulsant action, and preservation of memory from alcoholic damage in adult zebrafish. Molecular docking simulations showed that petrosamine exhibited better specificity for the binding site of the DZP agonist in $GABA_A$ receptors and also potential to inhibit CAII. The petrosamine/AChE

complex exerted a better energy value resulting in greater affinity with its respective interaction cavity, and thus expressing greater viability in the formation of the complex. It is worth highlighting that the biological activity related to the petrosamine compound is related to the non-competitive effect when compared with the crystallized inhibitor. This mechanism is favored by the pharmacokinetics of gradual access to the CNS, due to the alignment between apparent permeability and metabolic stability. Thus, the results confirm the pharmacological relevance of petrosamine as an anxiety inhibitor, as well as a memory prevention agent, allowing for the investigation of new therapeutic approaches. In addition, petrosamine shows intermediate reactivity with moderate HOMO-LUMO gap and high electrophilicity, where MEP and Fukui analyses consistently identify cationic nitrogens as electrophilic sites and O/Br atoms as nucleophilic regions.

Acknowledgements

Fundação Cearense de Apoio ao Desenvolvimento Científico e Tecnológico (FUNCAP), Conselho Nacional de Desenvolvimento Científico e Tecnológico (CNPq), Coordenação de Aperfeiçoamento de Pessoal de Nível Superior (CAPES) are acknowledged for financial support and scholarships, and Centro Nordestino de Aplicação e Uso da Ressonância Magnética Nuclear (CENAUREMN) for obtaining spectroscopic data.

Author's contributions

Joilna Alves da Silva: Supervision, laboratory test, writing, review and editing. Maria Kuerislene Amâncio Ferreira and Antônio Wlisses da Silva: Formal analysis, softwares, validation, and reviewed the manuscript. Jéssica Bezerra Maciel and Draulio Sales da Silva: Investigation – laboratory test. Emmanuel Siva Marinho and Márcia Machado Marinho: Investigation, *In silico* analysis, and writing - original draft. Francisco das Chagas Lima Pinto and Otília Deusdenia Loiola Pessoa and Kelma Maria dos Santos Pires Cavalcante: Conceptualization, methodology, and determined the molecular structures. Andreia Ferreira de Castro Gomes and Joana Ribeiro: Writing - original draft and aided in the analysis of the spectra. Mauro Macedo de Oliveira: DFT and Theoretical studies of reactivity investigation - original draft Carlos Emidio Sampaio Nogueira: DFT and Theoretical studies of reactivity investigation - original draft and Jane Eire Silva Alencar de Menezes and Hélcio Silva dos Santos: Project administration and writing – review and editing.

Funding Helcio Silva dos Santos acknowledges financial support from CNPq (Grant 306008/2022-0) and FUNCAP-INTERNATIONALIZATION (Grant ITR-0214-00060.01.00/23). Carlos Emidio Sampaio Nogueira acknowledges the Ceará Foundation for Scientific and Technological Development (FUNCAP, grant #BP6-0241-00116.01.00/25) for support and funding. Otília Deusdênia Loiola Pessoa acknowledges financial support from CNPq Universal (Grant 304817/2025-2).

Data Availability The data that support the findings of this study are available from the corresponding author upon reasonable request.

Ethical approval

The bioassays were performed in accordance with the Ethical Principles of Animal Experimentation and were approved by the Ethics Committee for the Use of Animals (CEUA) of the State University of Ceará (04983945/2021).

Declarations

Competing interest The authors declare no known financial conflicts of interest or personal relationships that could have influenced the work described in this paper.

References

1. Martins A, Vieira H, Gaspar H, Santos S (2014) Marketed marine natural products in the pharmaceutical and cosmeceutical industries: tips for success. Mar Drugs 12(2): 1066–1101. https://doi.org/10.3390/md12021066

2. Newman DJ, Cragg GM (2016) Natural Products as Sources of New Drugs from 1981 to 2014. J Nat Prod 79(3):629–661. https://doi.org/10.1021/acs.jnatprod.5b01055

3. Carroll AR, Copp BR, Davis RA, Keyzers RA, Prinsep MR (2019) Marine natural products. Nat Prod Rep 36:122–173. https://doi.org/10.1039/C8NP00092A

4. Mayer AMS, Rodríguez AD, Taglialatela-Scafati O, Fusetani N (2013) Marine pharmacology in 2009-2011: marine compounds with antibacterial, antidiabetic, antifungal, anti-inflammatory, antiprotozoal, antituberculosis, and antiviral activities; affecting the immune and nervous systems, and other miscellaneous mechanisms of action. Mar Drugs 11(7):2510–2573. https://doi.org/ 10.3390/md11072510

5. Lindequist U (2016) Marine-Derived Pharmaceuticals - Challenges and Opportunities. Biomol Ther 24(6):561–571. https://doi.org/ 10.4062/biomolther.2016.181

6. Jiménez C (2018) Marine natural products in medicinal chemistry. ACS Med Chem Lett, 9(10): 959–961. https://doi.org/10.1021/acsmedchemlett.8b00368

7. Lima E, Medeiros J (2022) Marine organisms as alkaloid biosynthesizers of potential anti-Alzheimer agents. Mar Drugs 20(1):75. https://doi.org/10.3390/md20010075

8. Lordan S, Ross RP, Stanton C (2011) Marine bioactives as functional food ingredients: potential to reduce the incidence of chronic diseases. Mar Drugs 9(6): 1056–1100. https://doi.org/ 10.3390/md9061056

9. Leal MC, Madeira C, Brandão CA, Puga J, Calado R (2012) Bioprospecting of marine invertebrates for new natural products - A chemical and zoogeographical perspective. Molecules 17(8): 9842–9854. https://doi.org/ 10.3390/molecules17089842

10. Hamed I, Özogul F, Özogul Y, Regenstein JM (2015) Marine bioactive compounds and their health benefits: a review. Compr Rev Food Sci Food Saf 14(4): 446–465. https://doi.org/ 10.1111/1541-4337.12136

11. Blunt JW, Carroll AR, Copp BR, Davis RA, Keyzers RA, Prinsep MR (2018) Marine natural products. Nat Prod Rep 35(1): 8–53. https://doi.org/ 10.1039/c7np00052a

12. Ryu B, Kim SK (2013) Potential beneficial effects of marine peptide on human neuron health. Curr Protein Pept Sci 14(3): 173–176. https://doi.org/ 10.2174/13892037113149990043

13. Choi DY, Choi H (2015) Natural products from marine organisms with neuroprotective activity in the experimental models of Alzheimer's disease, Parkinson's disease and ischemic brain stroke: their molecular targets and action mechanisms. Arch Pharm Res 38(2):139–170. https://doi.org/ 10.1007/s12272-014-0503-5

14. Guimarães PL, Tavares DQ, Carrião GS, Oliveira MEH, Oliveira CR (2023) Potential of marine compounds in the treatment of neurodegenerative diseases: a review. Braz J Biol 83:e266795. https://doi.org/10.1590/1519-6984.266795

15. Huynh TV, Davis AA, Ulrich JD, Holtzman DM (2017) Apolipoprotein E and Alzheimer's disease: the influence of apolipoprotein E on amyloid-β and other amyloidogenic proteins. J Lipid Res 58(5): 824–836. https://doi.org/ 10.1194/jlrR075481

16. Ribeiro HF, Dos Santos JSF, De Souza JN (2021) Early-onset Alzheimer's Disease (EOAD): neuropathological characteristics and associated genetic variants. Rev Neuropsiquiatr 84(2):113–127. https://doi.org/10.20453/rnp.v84i2.3998

17. Kumar A, Singh A, Ekavali (2015) A review on Alzheimer's disease pathophysiology and its management: an update. Pharmacol Rep, 67(2): 195–203. https://doi.org/ 10.1016/j.pharep.2014.09.004

18. Dai MH, Zheng H, Zeng LD, Zhang Y (2018) The genes associated with early-onset Alzheimer's disease. Oncotarget 9(19):15132–15143. https://doi.org/ 10.18632/oncotarget.23738

19. Sharma K (2019) Cholinesterase inhibitors as Alzheimer's therapeutics (Review). Mol Med Rep 20(2):1479–1487. https://doi.org/10.3892/mmr.2019.10374

20. Nukoolkarn VS, Saen-oon S, Rungrotmongkol T, Hannongbua S, Ingkaninan K, Suwanborirux K (2008) Petrosamine, a potent anticholinesterase pyridoacridine alkaloid from a Thai marine sponge *Petrosia* n. sp. Bioorg Med Chem 16(13): 6560–6567. https://doi.org/10.1016/j.bmc.2008.05.027

21. Konrath EL, Passos CDS, Klein-Júnior LC, Henriques AT (2013) Alkaloids as a source of potential anticholinesterase inhibitors for the treatment of Alzheimer's disease. J Pharm Pharmacol 65(12): 1701–1725. https://doi.org/ 10.1111/jphp.12090

22. Gartshore CJ, Wang X, Su Y, Molinski TF (2023) Petrosamine revisited. Experimental and computational investigation of solvatochromism, tautomerism and free energy landscapes of a pyridoacridinium quaternary salt. Mar Drugs 21(8): 446. https://doi.org/ 10.3390/md21080446

23. Mambro LD, Souza NVD, Silva WMB (2022) Activity of Acetylcholinesterase inhibitor Alkaloids in the treatment of Alzheimer's Disease: a systematic review. J. Health Biol Sci 10(1):1–10.

24. Pákáski M, Kálmán J (2008) Interactions between the amyloid and cholinergic mechanisms in Alzheimer's disease. Neurochem Int 53(5):103–111. https://doi.org/ 10.1016/j.neuint.2008.06.005

25. Ferreira-Vieira TH, Guimaraes IM, Silva FR, Ribeiro FM (2016) Alzheimer's disease: targeting the cholinergic system. Curr Neuropharmacol 14(1):101–115. https://doi.org/10.2174/1570159x13666150716165726

26. Santana S, Rico EP, Burgos JS (2012) Can zebrafish be used as animal model to study Alzheimer's disease? Am J Neurodegener Dis 1(1):32–48.

27. Silveira TR, Schneider AC, Hammes TO (2012) *Zebrafish*: modelo consagrado para estudos de doenças humanas. Cienc Cult 64(2):4–5. https://doi.org/ 10.21800/S0009-67252012000200002

28. Pan H, Zhang J, Wang Y, Cui K, Cao Y, Wang L, Wu Y (2019) Linarin improves the dyskinesia recovery in Alzheimer's disease *zebrafish* by inhibiting the acetylcholinesterase activity. Life Sci 222:112–116. https://doi.org/ 10.1016/j.lfs.2019.02.046

29. Teame T, Zhang Z, Ran C, Zhang H, Yang Y, Ding Q, Xie M, Gao C, Ye Y, Duan M, Zhou Z (2019) The use of *zebrafish* (*Danio rerio*) as biomedical models. Anim Front 9(3):68–77. https://doi.org/10.1093/af/vfz020

30. Siebel AM, Menezes FP, Capiotti KM, Kist LW, Da Costa Schaefer I, Frantz JZ, Bogo MR, Da Silva RS, Bonan CD (2015) Role of adenosine signaling on pentylenetetrazole-induced seizures in *zebrafish*. Zebrafish 12(2):127–136. https://doi.org/10.1089/zeb.2014.1004

31. Caramillo EM, Echevarria DJ (2017) Alzheimer's disease in the *zebrafish*: where can we take it? Behav Pharmacol 28(2):179–186.

https://doi.org/10.1097/FBP.0000000000000284

32. Koehler D, Williams FE (2018) Utilizing *zebrafish* and okadaic acid to study Alzheimer's disease. Neural Regen Res 13(9):1538–1541. https://doi.org/10.4103/1673-5374.237111

33. Ribeiro J, Araújo-Silva H, Fernandes M, da Silva JA, Pinto FDCL, Pessoa ODL, Santos HS, de Menezes JESA, Gomes AC. (2024) Petrosamine isolated from marine sponge *Petrosia* sp. demonstrates protection against neurotoxicity *in vitro* and *in vivo*. Natl Prod Bioprospect 14(1):16. https://doi.org/10.1007/s13659-024-00439-x

Marnielle Rodrigues Coutinho, Antonio Wlisses da Silva, Larissa Santos Oliveira et al (2023).,A Mixture of α, β-amyrin Causes Anxiolytic, Sedative, and Anticonvulsant Behavior without Impairing Memory in Adult Zebrafish., Journal of Veterinary Medicine and Research
34. OECD (2019) Test No. 203: Fish Acute Toxicity Test pp.24. https://doi.org/10.1787/9789264069961-e

35. Romão, I. C., Alves, A. M. B., de Sousa Silva, T., Marinho, M. M., Marinho, E. S., Rocha, M. N., ... & Dos Santos, H. S. (2025). Neuropharmacological evaluation of hydralazine hydrazone derivatives: Synthesis, In silico, and zebrafish studies. Biochemical and Biophysical Research Communications, 152728.

36. Ferreira MKA, da Silva AW, Dos Santos Moura AL, Sales KVB, Marinho EM, do Nascimento Martins Cardoso J, Marinho MM, Bandeira PN, Magalhães FEA, Marinho ES, de Menezes JESA, Dos Santos HS (2021) Chalcones reverse the anxiety and convulsive behavior of adult *zebrafish*. Epilepsy Behav 117:107881. https://doi.org/10.1016/j.yebeh.2021.107881

37. Ferreira MKA, da Silva AW, Silva FCO, Holanda CLA, Barroso SM, Lima JDR, Vieira Neto AE, Campos AR, Bandeira PN, Dos Santos HS, de Lemos TLG, Siqueira SMC, Magalhães FEA, de Menezes JESA (2019) Anxiolytic-like effect of chalcone N-{(4′-[(E)-3-(4-fluorophenyl)-1-(phenyl) prop-2-en-1-one]} acetamide on adult *zebrafish* (*Danio rerio*): involvement of the GABAergic system. Behav Brain Res 374:111871. https://doi.org/10.1016/j.bbr.2019.03.040

38. Ferreira MKA, da Silva AW, Silva FCO, Vieira Neto AE, Campos AR, Alves Rodrigues Santos SA, Rodrigues Teixeira AM, da Cunha Xavier J, Bandeira PN, Sampaio Nogueira CE, de Brito DHA, Rebouças EL, Magalhães FEA, de Menezes JESA, Dos Santos HS (2020) Anxiolytic-like effect of chalcone N-{4'[(2E)-3-(3-nitrophenyl)-1-(phenyl)prop-2-en-1-one]} acetamide on adult *zebrafish* (*Danio rerio*): involvement of the 5-HT system. Biochem Biophys Res Commun 526(2):505–511. https://doi.org/10.1016/j.bbrc.2020.03.129

39. Guedes JM, Ferreira MKA, Oliveira LS, da Silva AW, de Menezes JESA, Bandeira PN, Teixeira AMR, Marinho EM, Marinho MM, Marinho ES, Dos Santos HS (2023) Anxiolytic-like effect in adult *zebrafish* (*Danio rerio*) through GABAergic system and molecular docking study of chalcone (E)-1-(2-hydroxy-3,4,6-trimethoxyphenyl)-3-(4-methoxyphenyl)prop-2-en-1-one. Biointerface research in applied chemistry 13(1):15. https://doi.org/10.33263/BRIAC131.015

40. Mendes FRS, Wlisses da Silva A, Amâncio Ferreira MK, de Lima Rebouças E, Marinho EM, Marinho MM, Bandeira PN, Rodrigues Teixeira AM, Silva Alencar de Menezes JE, Alves

de Siqueira E, Róseo Paula Pessoa Bezerra de Menezes R, Marinho ES, Silva Dos Santos H (2022) $GABA_A$ receptor participation in anxiolytic and anticonvulsant effects of (E)-3-(furan-2-yl)-1-(2hydroxy-3,4,6-trimethoxyphenyl)prop-2-en-1-one in adult *zebrafish*. Neurochem Int 155:105303. https://doi.org/10.1016/j.neuint.2022.105303

41. Franscescon F, Müller TE, Bertoncello KT, Rosemberg DB (2020) Neuroprotective role of taurine on MK-801-induced memory impairment and hyperlocomotion in *zebrafish*. Neurochem Int 135:104710. https://doi.org/10.1016/j.neuint.2020.104710

42. Luchiari AC, Salajan DC, Gerlai R (2015) Acute and chronic alcohol administration: effects on performance of zebrafish in a latent learning task. Behav Brain Res, 282:76-83. https://10.1016/j.bbr.2014.12.013

43. Halgren TA (1996) Merck molecular force field. I. Basis, form, scope, parameterization, and performance of MMFF94. J Comput Chem 17(5-6):490–519. https://doi.org/10.1002/(SICI)1096987X(199604)17:5/6<490::AID-JCC1>3.0.CO;2-P

44. Lucio, F. N., Gomes, A. O., Bandeira, P. N., Ferreira, M. K., Ribeiro, W. H., Romão, I. C., ... & dos Santos, H. S. (2025). Synthesis, characterization, anxiolytic and anticonvulsant activity, DFT, molecular docking, DMPK studies of chalcone derived from maleic anhydride. Journal of Molecular Structure, 1322, 140466.

45. Masiulis S, Desai R, Uchański T, Serna Martin I, Laverty D, Karia D, Malinauskas T, Zivanov J, Pardon E, Kotecha A, Steyaert J, Miller KW, Aricescu AR (2019) $GABA_A$ receptor signalling mechanisms revealed by structural pharmacology. Nature 565(7740):454–459. https://doi.org/10.1038/s41586-018-0832-5

46. Trott O, Olson AJ (2010) AutoDock Vina: improving the speed and accuracy of docking with a new scoring function, efficient optimization, and multithreading. J Comput Chem 31(2):455–461. https://doi.org/10.1002/jcc.21334

47. Marinho EM, Batista de Andrade Neto J, Silva J, Rocha da Silva C, Cavalcanti BC, Marinho ES, Nobre Júnior HV (2020) Virtual screening based on molecular docking of possible inhibitors of Covid-19 main protease. Microb Pathog 148: 104365. https://doi.org/10.1016/j.micpath.2020.104365

48. MarvinSketh, Marvin was used for drawing, displaying and characterizing chemical structures, substructures and reactions, 2019.

49. Avery P, Ludowieg H, Autschbach J, Zurek E (2018) Extended hückel calculations on solids using the Avogadro Molecular Editor and visualizer. J Chem Educ 95(2): 331–337. https://doi.org/10.1021/acs.jchemed.7b00698

50. Hanif AU, Lukis P, Fadlan A (2020) Pengaruh minimisasi energi MMFF94 dengan MarvinSketch dan open Babel PyRx pada penambatan molekular turunan oksindola tersubstitusi. Alchemy: Journal of Chemistry, 8(2):33–40. https://doi.org/10.18860/al.v8i2.10481

51. De Oliveira VM, Da Rocha MN, Roberto CHA, Lúcio FNM, Marinho MM, Marinho ES, De Morais SM (2024) Insights of structure-based virtual screening and MPO-based SAR

analysis of berberine-benzimidazole derivatives against Parkinson disease. J Mol Struct, 1302:137453. https://doi.org/10.1016/j.molstruc.2023.137453

52. Burley SK, Berman HM, Kleywegt GJ, Markley JL, Nakamura H, Velankar S (2017) Protein Data Bank (PDB): The single global macromolecular structure archive. Methods Mol Biol, 1607:627–641. https://doi.org/10.1007/978-1-4939-7000-1_26

53. Cheung J, Rudolph MJ, Burshteyn F, Cassidy MS, Gary EN, Love J, Franklin MC, Height JJ (2012) Structures of human acetylcholinesterase in complex with pharmacologically important ligands. J Med Chem, 55(22):10282-6. https://doi.org/ 10.1021/jm300871x

54. Pettersen EF, Goddard TD, Huang CC, Meng EC, Couch GS, Croll TI, Morris JH, Ferrin TE (2021) UCSF ChimeraX: Structure visualization for researchers, educators, and developers. Protein Sci, 30(1):70–82. https://doi.org/10.1002/pro.3943

55. Tan A, Almaz Z (2022) Synthesis, investigation of the cholinesterase inhibitory activities and *in silico* studies of some novel N-substituted phthalimide derivatives. J Iran Chem Soc, 19(7):2833–2844. https://doi.org/10.1007/s13738-022-02492-0.

56. Huey R, Morris GM, Forli S (2012) Using AutoDock 4 and AutoDock Vina with AutoDockTools: A tutorial. Scripps Res. Inst. Mol. Graph. Lab, 10550, 1000.

57. Gasteiger J, Marsili M (1978) A new model for calculating atomic charges in molecules. Tetrahedron lett, 19(34):3181–3184. https://doi.org/10.1016/S0040-4039(01)94977-9

58. Morris GM, Huey R, Lindstrom W, Sanner MF, Belew RK, Goodsell DS, Olson AJ (2009) AutoDock4 and AutoDockTools4: Automated docking with selective receptor flexibility. J Comput Chem, 30(16):2785-2791. https://doi.org/10.1002/jcc.21256

59. Wager TT, Hou X, Verhoest PR, Villalobos A (2010) Moving beyond rules: the development of a central nervous system multiparameter optimization (CNS MPO) approach to enable alignment of druglike properties. ACS Chem Neurosci 1(6):435–449. https://doi.org/10.1021/cn100008c

60. Johnson TW, Dress KR, Edwards M (2009) Using the golden triangle to optimize clearance and oral absorption. Bioorg Med Chem Lett 19(19):5560–5564. https://doi.org/10.1016/j.bmcl.2009.08.045

61. Ritchie TJ, Ertl P, Lewis R (2011) The graphical representation of ADME-related molecule properties for medicinal chemists. Drug Discov Today 16(1-2):65–72. https://doi.org/10.1016/j.drudis.2010.11.002

62. Rocha MN, Marinho MM, Santos HS, Marinho ES, Junior JI, Rosas JF, Coutinho HDM (2023) Structure-based virtual screening of new antitumor natural berberines: bioactivity against pancreas cancer by HIF1 inhibition effect. J Mol Struct 1294(1):136508. https://doi.org/ 10.1016/j.molstruc.2023.136508

63. Maximino C, De Brito TM, Batista AWS, Herculano AM, Morato S, Gouveia A (2010) Measuring anxiety in *zebrafish*: a critical review. Behav Brain Res 214(2):157–171.

https://doi.org/10.1016/j.bbr.2010.05.031

64. Gebauer DL, Pagnussat N, Piato AL, Schaefer IC, Bonan CD, Lara DR (2011) Effects of anxiolytics in *zebrafish*: similarities and differences between benzodiazepines, buspirone and ethanol. Pharmacol Biochem Behav 99(3):480–486. https://doi.org/ 10.1016/j.pbb.2011.04.021

65. Cachat JM, Canavello PR, Elegante MF, Bartels BK, Elkhayat SI, Hart PC, Tien AK, Tien DH, Beeson E, Mohot S, Laffoon AL, Stewart AM, Gaikwad S, Wong K, Haymore W, Kalueff AV (2010) Modeling stress and anxiety in *zebrafish*. Neuromethods, 52:73–88. https://doi.org/10.1007/978-1-60761-922-2_3

66. Gerlai R (2003) *Zebrafish*: an uncharted behavior genetic model. Behav Genet 33(5): 461–468. https://doi.org/ 10.1023/a:1025762314250

67. Blaser R, Gerlai R (2006) Behavioral phenotyping in *zebrafish*: comparison of three behavioral quantification methods. Behavior Research Methods 38(3):456–469. https://doi.org/10.3758/bf03192800

68. Goode TD, Maren S (2014) Animal models of fear relapse. ILAR J 55(2):246–258. https://doi.org/10.1093/ilar/ilu008

69. Calhoon GG, Tye KM (2015) Resolving the neural circuits of anxiety. Nat Neurosci, 18(10):1394–1404. https://doi.org/10.1038/nn.4101

70. Abreu MS, Giacomini ACVV, Demin KA, Galstyan DS, Zabegalov KN, Kolesnikova TO, Amstislavskaya TG, Strekalova T, Petersen EV, Kalueff AV (2021) Unconventional anxiety pharmacology in zebrafish: Drugs beyond traditional anxiogenic and anxiolytic spectra. Pharmacol Biochem Behav, 207:173205. https://doi.org/ 10.1016/j.pbb.2021.173205

71. Abreu MS, Koakoski G, Ferreira D, Oliveira TA, Rosa JG, Gusso D, Giacomini AC, Piato AL, Barcellos LJ (2014) Diazepam and fluoxetine decrease the stress response in *zebrafish*. PLoS ONE 9(7):e103232. https://doi.org/10.1371/journal.pone.0103232

72. MacRae CA, Peterson RT (2015) *Zebrafish* as tools for drug discovery. Nat Rev Drug Discov 14(10):721–731. https://doi.org/10.1038/nrd4627

73. Howe K, Clark MD, Torroja CF, Torrance J, Berthelot C, Muffato M, Collins JE, Humphray S, McLaren K, Matthews L, McLaren S, Sealy I, Caccamo M, Churcher C, Scott C, Barrett JC, Koch R, Rauch GJ, White S, Chow W, Kilian B, Quintais LT, Guerra-Assunção JA, Zhou Y, Gu Y, Yen J, Vogel JH, Eyre T, Redmond S, Banerjee R, Chi J, Fu B, Langley E, Maguire SF, Laird GK, Lloyd D, Kenyon E, Donaldson S, Sehra H, Almeida-King J, Loveland J, Trevanion S, Jones M, Quail M, Willey D, Hunt A, Burton J, Sims S, McLay K, Plumb B, Davis J, Clee C, Oliver K, Clark R, Riddle C, Elliot D, Threadgold G, Harden G, Ware D, Begum S, Mortimore B, Kerry G, Heath P, Phillimore B, Tracey A, Corby N, Dunn M, Johnson C, Wood J, Clark S, Pelan S, Griffiths G, Smith M, Glithero R, Howden P, Barker N, Lloyd C, Stevens C, Harley J, Holt K, Panagiotidis G, Lovell J, Beasley H, Henderson C, Gordon D, Auger K, Wright D, Collins J, Raisen C, Dyer L, Leung K, Robertson L, Ambridge K, Leongamornlert D, McGuire S, Gilderthorp R, Griffiths C, Manthravadi D, Nichol S, Barker G, Whitehead S, Kay M, Brown J, Murnane C, Gray E, Humphries M, Sycamore N, Barker D, Saunders D, Wallis J, Babbage A, Hammond S, Mashreghi-Mohammadi M, Barr L, Martin S,

Wray P, Ellington A, Matthews N, Ellwood M, Woodmansey R, Clark G, Cooper J, Tromans A, Grafham D, Skuce C, Pandian R, Andrews R, Harrison E, Kimberley A, Garnett J, Fosker N, Hall R, Garner P, Kelly D, Bird C, Palmer S, Gehring I, Berger A, Dooley CM, Ersan-Ürün Z, Eser C, Geiger H, Geisler M, Karotki L, Kirn A, Konantz J, Konantz M, Oberländer M, Rudolph-Geiger S, Teucke M, Lanz C, Raddatz G, Osoegawa K, Zhu B, Rapp A, Widaa S, Langford C, Yang F, Schuster SC, Carter NP, Harrow J, Ning Z, Herrero J, Searle SM, Enright A, Geisler R, Plasterk RH, Lee C, Westerfield M, de Jong PJ, Zon LI, Postlethwait JH, Nüsslein-Volhard C, Hubbard TJ, Roest Crollius H, Rogers J, Stemple DL (2013) The *zebrafish* reference genome sequence and its relationship to the human genome. Nature 496(7446):498–503. https://doi.org/10.1038/nature12111

74. Stewart A, Gaikwad S, Kyzar E, Green J, Roth A, Kalueff AV (2012) Modeling anxiety using adult *zebrafish*: a conceptual review. Neuropharmacology 62(1):135–143. https://doi.org/10.1016/j.neuropharm.2011.07.037

75. Kysil EV, Meshalkina DA, Frick EE, Echevarria DJ, Rosemberg DB, Maximino C, Lima MG, Abreu MS, Giacomini AC, Barcellos LJG, Song C, Kalueff AV (2017) Comparative analyses of *zebrafish* anxiety-like behavior using conflict-based novelty tests. Zebrafish 14(3):197–208. https://doi.org/10.1089/zeb.2016.1415

76. Wang L, Jiang W, Lin Q, Zhang Y, Zhao C (2016) DNA methylation regulates gabrb2 mRNA expression: developmental variations and disruptions in L-methionine-induced *zebrafish* with schizophrenia-like symptoms. Genes Brain Behav 15(8):702–710. https://doi.org/10.1111/gbb.12315

77. Lakstygal AM, de Abreu MS, Kalueff AV (2018) *Zebrafish* models of epigenetic regulation of CNS functions. Brain Res Bull 142:344–351. https://doi.org/ 10.1016/j.brainresbull.2018.08.022

78. Cheresiz SV, Volgin AD, Kokorina Evsyukova A, Bashirzade AAO, Demin KA, de Abreu MS, Amstislavskaya TG, Kalueff AV (2020) Understanding neurobehavioral genetics of *zebrafish*. J Neurogenet 34(2):203–215. https://doi.org/10.1080/01677063.2019

79. Giacomini ACVV, Abreu MS, Giacomini LV, Siebel AM, Zimerman FF, Rambo CL, Mocelin R, Bonan CD, Piato AL, Barcellos LJG (2016a) Fluoxetine and diazepam acutely modulate stress induced-behavior. Behav Brain Res 296:301–310. https://doi.org/10.1016/j.bbr.2015.09.027

80. Giacomini ACVV, Abreu MS, Zanandrea R, Saibt N, Friedrich MT, Koakoski G, Gusso D, Piato AL, Barcellos LJG (2016b) Environmental and pharmacological manipulations blunt the stress response of *zebrafish* in a similar manner. Sci Rep 6(1):28986. https://doi.org/10.1038/srep28986

81. Marcon M, Mocelin R, Benvenutti R, Costa T, Herrmann AP, de Oliveira DL, Koakoski G, Barcellos LJG, Piato A (2018) Environmental enrichment modulates the response to chronic stress in *zebrafish*. J Exp Biol 221(4):jeb176735. https://doi.org/10.1242/jeb.176735

82. Lee CJ, Paull GC, Tyler CR (2019) Effects of environmental enrichment on survivorship, growth, sex ratio and behaviour in laboratory maintained *zebrafish Danio rerio*. J Fish Biol 94(1):86–95. https://doi.org/10.1111/jfb.13865

83. Farzaei MH, Bahramsoltani R, Rahimi R, Abbasabadi F, Abdollahi M (2016) A systematic review of plant-derived natural compounds for anxiety disorders. Curr Top Med Chem 16(17):1924–1942. https://doi.org/10.2174/1568026616666160204121039

84. Phootha N, Yongparnichkul N, Fang Z, Gan RY, Zhang P (2022) Plants and phytochemicals potentials in tackling anxiety: a systematic review. Phytomed Plus 2(4):100375. https://doi.org/10.1016/j.phyplu.2022.100375

85. Wu C, Sun D (2015) GABA receptors in brain development, function, and injury. Metab Brain Dis 30(2):367–379. https://doi.org/10.1007/s11011-014-9560-1

86. Lee SE, Lee Y, Lee GH (2019) The regulation of glutamic acid decarboxylases in GABA neurotransmission in the brain. Arch Pharm Res 42(12):1031–1039. https://doi.org/10.1007/s12272-019-01196-z

87. Goodman AC, Wong RY (2020) Differential effects of ethanol on behavior and $GABA_A$ receptor expression in adult *zebrafish* (*Danio rerio*) with alternative stress coping styles. Sci Rep 10(1):13076. https://doi.org/10.1038/s41598-020-69980-2

88. Banote RK, Koutarapu S, Chennubhotla KS, Chatti K, Kulkarni P (2013) Oral gabapentin suppresses pentylenetetrazole-induced seizure-like behavior and cephalic field potential in adult *zebrafish*. Epilepsy Behav 27(1):212–219. https://doi.org/10.1016/j.yebeh.2013.01.018

89. Berghmans S, Hunt J, Roach A, Goldsmith P (2007) *Zebrafish* offer the potential for a primary screen to identify a wide variety of potential anticonvulsants. Epilepsy Res 75(1):18–28. https://doi.org/10.1016/j.eplepsyres.2007.03.015

90. Choo BKM, Kundap UP, Johan Arief MFB, Kumari Y, Yap JL, Wong CP, Othman I, Shaikh MF (2019) Effect of newer anti-epileptic drugs (AEDs) on the cognitive status in pentylenetetrazol induced seizures in a *zebrafish* model. Prog Neuropsychopharmacol Biol Psychiatry 92:483–493. https://doi.org/10.1016/j.pnpbp.2019.02.014

91. Yusuf D, Davis AM, Kleywegt GJ, Schmitt S (2008) An alternative method for the evaluation of docking performance: RSR vs RMSD. J Chem Inf Model 48(7):1411–1422. https://doi.org/10.1021/ci800084x

92. Shityakov S, Förster C (2014) In silico predictive model to determine vector-mediated transport properties for the blood-brain barrier choline transporter. Adv Appl Bioinform Chem 7:23-36. https://doi.org/10.2147/AABC.S63749

93. Maresca A, Temperini C, Vu H, Pham NB, Poulsen SA, Scozzafava A, Quinn RJ, Supuran CT (2009) Non-zinc mediated inhibition of carbonic anhydrases: coumarins are a new class of suicide inhibitors. J Am Chem Soc 131(8):3057–3062. https://doi.org/10.1021/ja809683v

94. Wager TT, Hou X, Verhoest PR, Villalobos A (2016) Central nervous system multiparameter optimization desirability: application in drug discovery. ACS Chem Neurosci 7(6):767–775. https://doi.org/10.1021/acschemneuro.6b00029

95. Pettersson M, Hou X, Kuhn M, Wager TT, Kauffman GW, Verhoest PR (2016) Quantitative assessment of the impact of fluorine substitution on P-Glycoprotein (P-gp) mediated efflux, permeability, lipophilicity, and metabolic stability. J Med Chem 59(11):5284–5296. https://doi.org/10.1021/acs.jmedchem.6b00027

96. Van de Waterbeemd H, Gifford E (2003) ADMET *in silico* modelling: towards prediction paradise?. Nat Rev Drug Discov 2(3):192–204. https://doi.org/10.1038/nrd1032

97. Oberhauser N, Nurisso A, Carrupt PA (2014) MLP Tools: a PyMOL plugin for using the molecular lipophilicity potential in computer-aided drug design. J Comput Aided Mol Des 28(5):587–596. https://doi.org/10.1007/s10822-014-9744-0

98. Ertl P (2007) Polar Surface Area, In: Mannhold, R. Ed., Molecular Drug Properties, Wiley-VCH, Heidelberg pp. 111-126. https://dx.doi.org/10.1002/9783527621286.ch5

99. Didziapetris R, Japertas P, Avdeef A, Petrauskas A (2003) Classification analysis of P-glycoprotein substrate specificity. J Drug Target 11(7):391–406. https://doi.org/10.1080/10611860310001648248

100. Yu K, Geng X, Chen M, Zhang J, Wang B, Ilic K, Tong W (2014) High daily dose and being a substrate of cytochrome P450 enzymes are two important predictors of drug-induced liver injury. Drug Metab Dispos 42(4):744–750. https://doi.org/10.1124/dmd.113.056267

101. Zheng M, Luo X, Shen Q, Wang Y, Du Y, Zhu W, Jiang H (2009) Site of metabolism prediction for six biotransformations mediated by cytochromes P450. Bioinformatics 25(10):1251–1258. https://doi.org/10.1093/bioinformatics/btp140

102. Hughes TB, Miller GP, Swamidass SJ (2015) Modeling epoxidation of drug-like molecules with a deep machine learning network. ACS Cent Sci 1(4):168–180. https://doi.org/10.1021/acscentsci.5b00131

103. Marshall KM, Matsumoto SS, Holden JA, Concepción GP, Tasdemir D, Ireland CM, Barrows LR (2003) The anti-neoplastic and novel topoisomerase II-mediated cytotoxicity of neoamphimedine, a marine pyridoacridine. Biochem Pharmacol 66(3):447–458. https://doi.org/10.1016/s0006-2952(03)00209-0

104. Bakrim S, Aboulaghras S, El Menyiy N, El Omari N, Assaggaf H, Lee LH, Montesano D, Gallo M, Zengin G, AlDhaheri Y. (2022) Phytochemical Compounds and Nanoparticles as Phytochemical Delivery Systems for Alzheimer's Disease Management. *Molecules* 27(24):9043. https://doi.org/10.3390/molecules27249043

105. Bry D, Banaigs B, Christophe L, Bontemps N (2011) New pyridoacridine alkaloids from the purple morph of the ascidian *Cystodytes dellechiajei*. Tetrahedron Lett 52(23):3041–3044. https://doi.org/10.1016/j.tetlet.2011.04.005

107. COHEN, M. H.; WASSERMAN, A. On the foundations of chemical reactivity theory. The Journal of Physical Chemistry A, v. 111, n. 11, p. 2229–2242, 2007.

108. KLOPMAN, G. Chemical reactivity and the concept of charge-and frontier-controlled reactions. Journal of the American Chemical Society, Washington, v. 90, n. 2, p. 223–234, 1968.

109. Chakraborty D, Chattaraj PK. Conceptual density functional theory based electronic structure principles. Chem Sci. 2021 Mar 31;12(18):6264-6279.

110. KOHN, Walter; SHAM, Lu Jeu. Self-consistent equations including exchange and correlation effects. Physical review, v. 140, n. 4A, p. A1133, 1965.

111. Chai, J.-D.; Head-Gordon, M. Long-range corrected hybrid density functionals with damped atom-atom dispersion corrections, Phys. Chem. Chem. Phys. 2008, 10, 6615-6620.

112. GEERLINGS, Paul; DE PROFT, Frank; LANGENAEKER, Wilfried. Conceptual density functional theory. Chemical reviews, v. 103, n. 5, p. 1793-1874, 2003.

113. OÑA, Ofelia B. et al. Atom and Bond Fukui Functions and Matrices: A Hirshfeld-I Atoms-in-Molecule Approach. ChemPhysChem, v. 17, n. 18, p. 2881-2889, 2016.

114. SABLON, Nick et al. Computing Fukui functions without differentiating with respect to electron number. II. Calculation of condensed molecular Fukui functions. The Journal of chemical physics, v. 126, n. 22, 2007.

115. Politzer P, Laurence PR, Jayasuriya K. Molecular electrostatic potentials: an effective tool for the elucidation of biochemical phenomena. Environ Health Perspect. 1985 Sep;61:191-202.

Supplementary Files

This is a list of supplementary files associated with this preprint. Click to download.

- Supplementarymaterial.doc